IEEE Access
Multidisciplinary ⋮ Rapid Review ⋮ Open Access Journal

Received 2 August 2022, accepted 9 September 2022, date of publication 19 September 2022, date of current version 26 September 2022.

Digital Object Identifier 10.1109/ACCESS.2022.3207768

RESEARCH ARTICLE

Electrodynamic Forces in a High Voltage Circuit Breakers With Tulip Contact System–FEM Simulations

MICHAŁ SZULBORSKI[1,2], SEBASTIAN ŁAPCZYŃSKI[1], ŁUKASZ KOLIMAS[1], AND MYKHAILO TYRYK[3]

[1]Institute of Electrical Power Engineering, Warsaw University of Technology, 00-662 Warsaw, Poland
[2]Symkom Sp. z o.o., Ansys Channel Partner, 02-639 Warsaw, Poland
[3]Faculty of Power and Aeronautical Engineering, Warsaw University of Technology, 00-665 Warszawa, Poland

Corresponding author: Michał Szulborski (mm.szulborski@gmail.com)

ABSTRACT Paper concerns the effects of electrodynamic forces that act on the contacts of the tulip contact system that is often implemented in high voltage circuit breakers. The high voltage circuit breaker often consists of two such systems. One of the systems is treated as an arcing one - made of tungsten coated elements. Capable of implementing the phenomenon of thermal-expansion. The second is made of one or two crown laces. The first system consists of a single piece of large mass, cut in such a way as to obtain the effect of increasing the contact surface. The second is a system, often of several dozen contacts, so as to increase the contact area and reduce the transition resistance. The main problem of actual validation through dynamic measurements (electrodynamic forces) is the specificity of the circuit breaker operation. The contact system is located directly in the switch chamber filled with CO_2 or SF_6 gas. Hence, tests under normal working conditions are very difficult - even impossible. Therefore, the authors proposed employment of FEM (Finite Element Method) in order to obtain values of electrodynamic forces acting on the contact system by executing the detailed 3D coupled simulation. The analysis of the results brought interesting conclusions that concerned operation of such contact layouts in short circuit conditions.

INDEX TERMS Electrodynamic forces, FEM, tulip contact, high voltage, circuit breakers.

I. INTRODUCTION

The formation of electrodynamic forces in the contacts of electrical devices is related to the flow of high currents, mostly short-circuit currents. Depending on the design of the contact system, the occurrence of electrodynamic forces is undesirable, as it can lead to welding of the contacts during electrodynamic bounces or even to their rupture and destruction. On the other hand, the electrodynamic recoil force is used to increase the speed of contact propagation in circuit breakers by employing appropriate loop shaping of the contact current paths. Due to the complexity concerning the occurrence of electrodynamic forces in contacts, in order to verify the structure in terms of resistance to electrodynamic contact bounces, tests are performed with the use of special devices under model conditions. Model systems for testing contact welding should reflect the real conditions in the circuit breakers to the greatest extent and should allow for adjustment of mechanical contact parameters, e.g. spring pressure. The phenomenon of electrodynamic bounce is revealed in two cases:

- when contact is closed during the flow of short-circuit current;
- at the moment of switching.

The phenomenon of electrodynamic contact bounce can lead to the formation of metallic bridges at the point of contact. It is caused by condensation of current streams which was shown in Figure 1 above. As a result of the high current flow at the point of contact, the contact material may evaporate. This creates additional forces and pressures greater than the generated electrodynamic forces, which can lead to the opening of the contacts and their damage by an electric arc.

The associate editor coordinating the review of this manuscript and approving it for publication was Giambattista Gruosso.

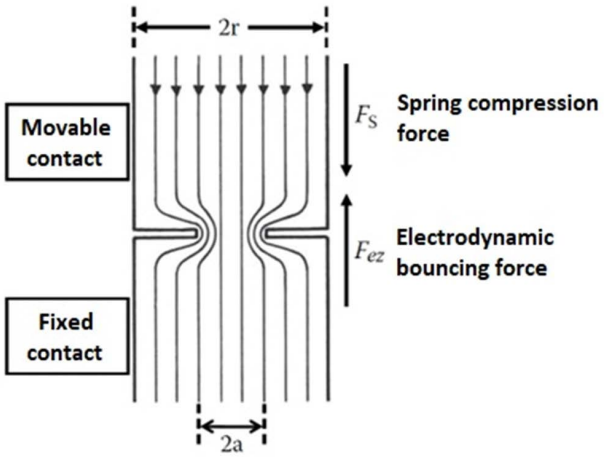

FIGURE 1. Generation of electrodynamic forces at the contact point caused by the condensation of current streams.

According to the complexity of the electrodynamic contact bouncing mechanism it is very hard to experimentally measure forces and phenomena occurring. Therefore authors propose to employ FEM in order to execute advanced coupled analysis and highlight values of electrodynamic forces and their influence that acts on high voltage circuit breaker tulip contact systems in two different versions. Moreover, this publication presents an approach for simulating electrodynamic forces in a tulip contact system that concerns the whole inner and outer crown not only one contactor (single lamella).

II. ANALYSIS OF ELECTRODYNAMIC FORCES PHENOMENA IN ELECTRICAL APPARATUSES

The phenomenon of electrodynamic contact bounce occurring in the contacts of high current electrical devices is related to the narrowing of the current lines at the point of the actual contact of conductors during the current flow. The microstructure of the contact surfaces is not perfectly even, there are specific current conduction zones in it, precisely illustrated below in the Figure 2.

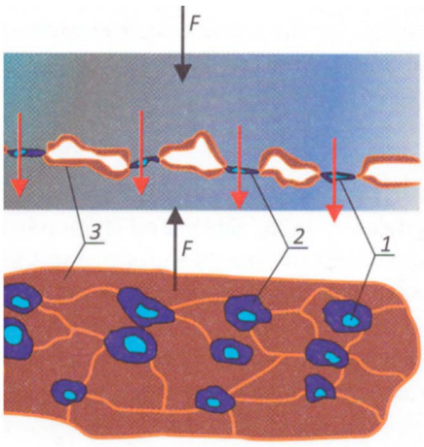

FIGURE 2. Conduction zones in the microstructure of contact surfaces; 1) electrically conductive zones, 2) semi-conductive zones - tunnel electric conduction, 3) non-conductive zones with coating layers [5].

When performing analytical calculations concerning the determination of electrodynamic contact bouncing forces that result in contacts abrupt repulsion, the main difficulty is determining the actual points of conductors contact. It is often the case that there are many zones of contact, which results in the formation of several parallel densities of the current lines as in the Figure 1 above. As a result, the electrodynamic contact bounce force is reduced. In the case of a single point of actual contact between the conductors surfaces, the force value can be determined from the dependency:

$$F_{ez} = 10^{-7} \cdot i^2 \cdot \ln\frac{D}{2a} \tag{1}$$

where: i is instantaneous current value; D is outer diameter of the contact and a is radius of the actual contact surface.

In the case of contacts with a cross-section other than cylindrical, e.g. rectangular, of the equivalent diameter (D) the circular cross-section is determined. An example may be rectangular contact strips for which in practice the equivalent diameter D is determined. In the case of frontal loop contacts, apart from the F_{ez} force, there is also a loop electrodynamic force F_{ep} resulting from the loop shape of the contact, which additionally increases the effect of electrodynamic bounce. In some constructions it is used to accelerate the opening velocity of moving contacts during short-circuit currents. An example of this type of solution with a contact system for a low voltage circuit breaker is shown in the Figure 3 below.

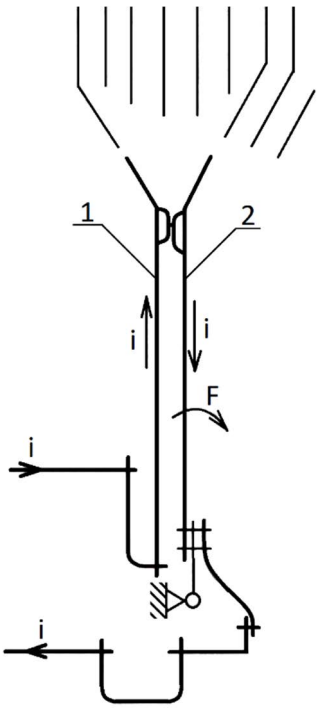

FIGURE 3. An example diagram of a LV switch contact, where the electrodynamic bounce force was used to accelerate the opening of the moving contact during the flow of short-circuit current.

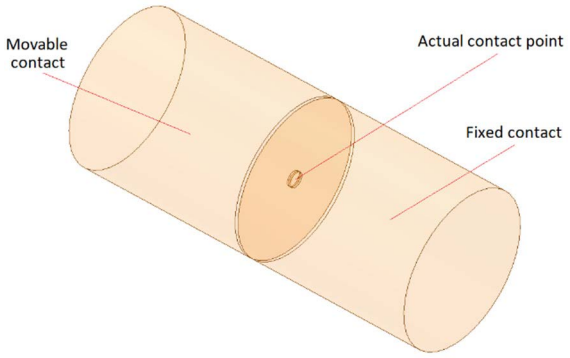

FIGURE 4. Initial 3D model of a contact geometry consisting of a movable and fixed contact.

The electrodynamic bouncing force between the contacts can be determined from the formula:

$$F_{ep} = 2 \cdot 10^{-7} \cdot i^2 \cdot \frac{l}{b} k_D \tag{2}$$

where: l, b are dimensions of the equivalent rectangular current loop of the contact, k_D is Dwight coefficient which value is depending on the cross-section of the contact arms.

It is assumed that the electrodynamic bouncing of the contacts starts when the electrodynamic force is greater than the values of the pressure springs which is expressed by relation (3):

$$F_e = F_{ez} + F_{ep} \geq F_s \tag{3}$$

where: F_s is contact spring pressure force.

In practice, it turns out that the propagation of the contacts and the appearance of an electric arc start already with the resultant electrodynamic force F_e lower than the pressure force of the springs pressing the contacts - F_s. This is due to the force generated by the rapid heating of the contact point and the explosive liquid decomposition of the formed metallic bridge. The extra force had impulse characteristics.

III. ELECTRODYNAMIC FORCES IN FEM SIMULATIONS

In order to determine the value of the electrodynamic force for the contact system, a 3D model was made for numerical analysis. The model was made for one actual point of surface contact. Initial stage of model geometry was shown in Figure 4 below.

After preparing the model and loading it into the Ansys Maxwell 3D environment, it was possible to assign boundary conditions, assign material properties and impose a current of 6 kA on the analyzed contact, in this case without a non-periodic component. Waveform of the short-circuit current in a single-point contact used during this analysis was shown in Figure 5 below.

The computational simulation of the short-circuit current flow through the contacts allowed to determine the current density at the actual point of contact and it was shown below in Figure 6.

As can be seen from the waveform in Figure 7 below, the interaction of the components in the Y direction is responsible for the repulsion of one contact from the other. In order to illustrate this phenomenon even better, the Y components of the two contacts are summarized on the waveform below. The presented forces in this case can lead to electrodynamic bounces in the case when the spring pressing the moving contact has a lower value than the sum of the forces presented as in equation (3) above and in the waveform in Figure 8 below.

In order to determine the vectors of the generated electrodynamic forces in the analyzed single-point contact, the results of calculations from Maxwell 3D were imported to the Ansys Transient Structural calculation module. On the basis of the performed analyses, it was possible to generate the values of the electrodynamic force vectors, which reached the highest value in the contraction of the contact, with the highest short-circuit current density.

Two components of electrodynamic forces can be distinguished from the analysis of electrodynamic forces in a contact system layout presented above:

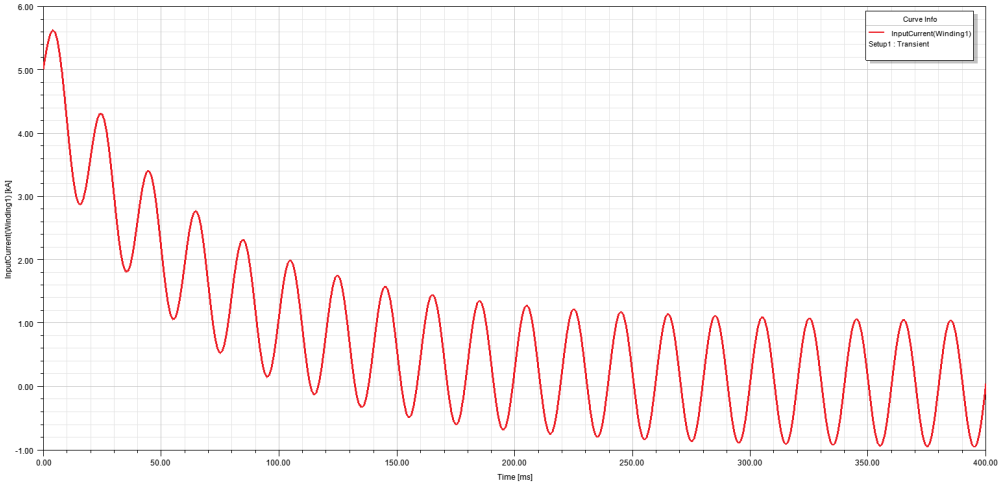

FIGURE 5. Short-circuit current waveform in a single-point contact layout—6 kA.

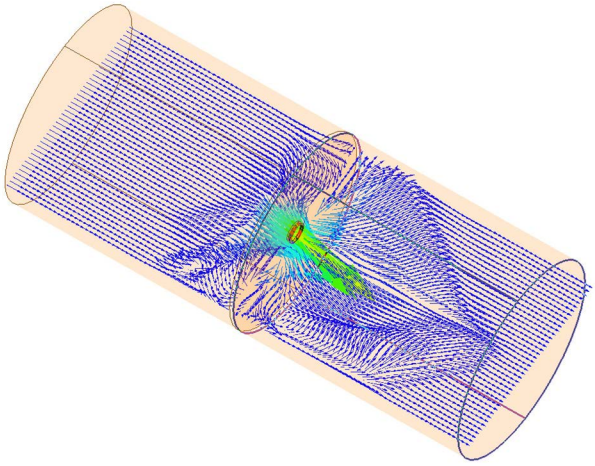

FIGURE 6. Distribution of the short-circuit current line flowing through a contact consisting of a movable and fixed contact with one point of actual contact.

- adial component,
- axial component.

Radial component of the generated electrodynamic forces causing compression of the contact material at the point of contact. Axial component of the resulting electrodynamic forces tending to break the contacts. The phenomenon from the analysis performed is illustrated in detail in the Figure 9 below.

The occurrence of electrodynamic forces in the contacts of electrical devices is a generally unfavorable phenomenon, which significantly reduces the contact pressure force, or at high values of the short-circuit current it leads to their abrupt opening. In order to prevent this phenomenon, electrodynamic force compensation systems are used. This is done by increasing the contact pressure force by applying the special cuts in the current paths or appropriate shaping of the current path inside an electrical apparatus, e.g. a circuit breaker. While current is flowing, forces are pressing the movable contacts or any contact elements to the fixed contact, compensating the electrodynamic bounce force. In tulip contacts, due to the uniform distribution of the contacts in relation to each other, with unidirectional current flow, the contacts are pressed against the pin, which in this case is a favorable phenomenon.

IV. INFLUENCE OF ELECTRODYNAMIC BOUNCES ON THE CONTACT WELDING

Due to the flow of short-circuit currents, electrodynamic forces influence in the contacts may result in bouncing and erosive changes on the contact surfaces. During the opening of the contacts, bridges of the molten metal may form, which may lead to permanent grafting of the connector contacts while the contacts are closing.

During the closing of the electrical device contacts, the movable contact collides with the fixed contact. The movable contact of the apparatus is influenced by the forces from the pressure spring of the connector, electrodynamic forces and forces from the generated intra-arcuate pressure (directed against the forces coming from the connector drive). After the contacts collide, the kinetic energy is converted into potential energy in the form of elastic stress in the movable contact of the switch, and then the potential energy is again converted into kinetic energy of the

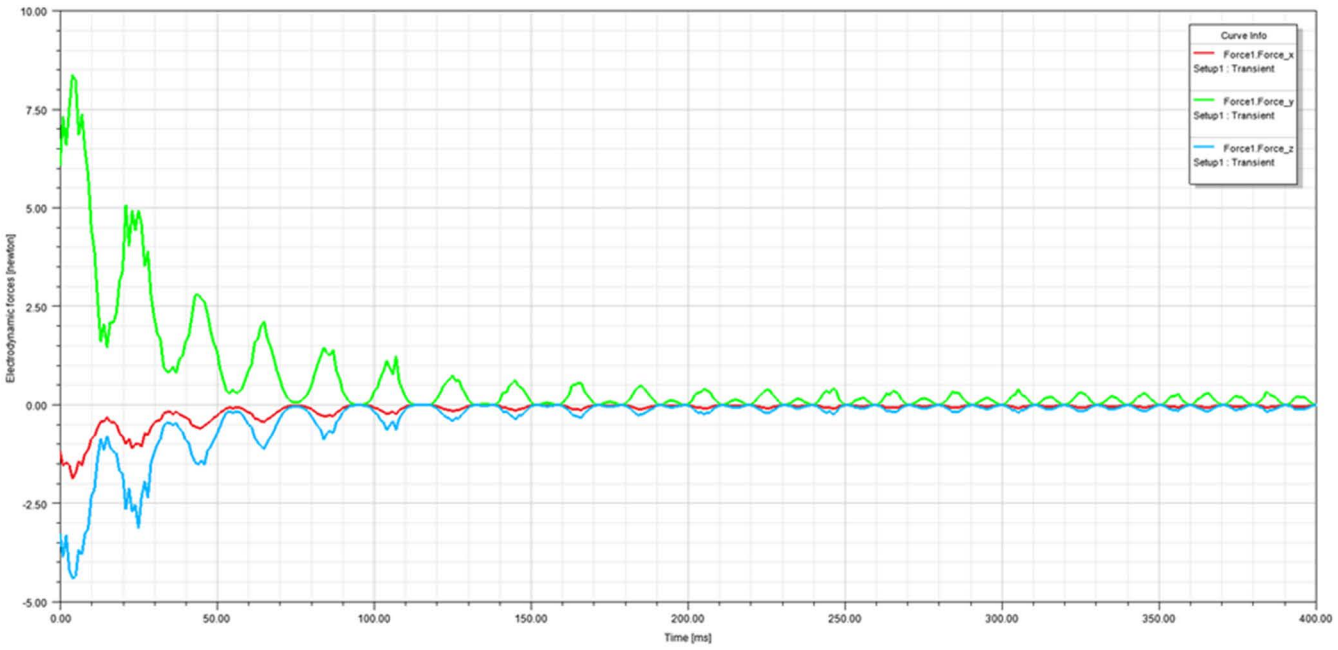

FIGURE 7. Determined *X*, *Y* and *Z* components of electrodynamic forces in a contact with one actual point of contact.

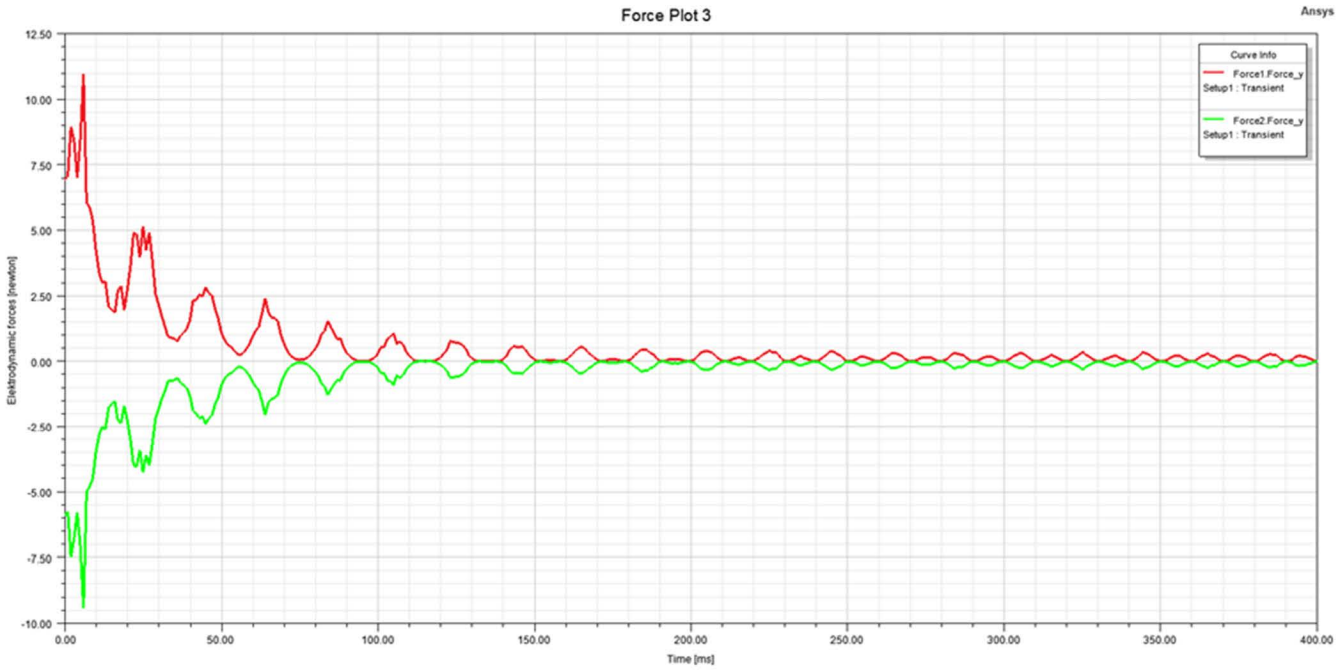

FIGURE 8. Determined *Y* components of the generated electrodynamic forces in the analyzed contact system with one actual point of contact.

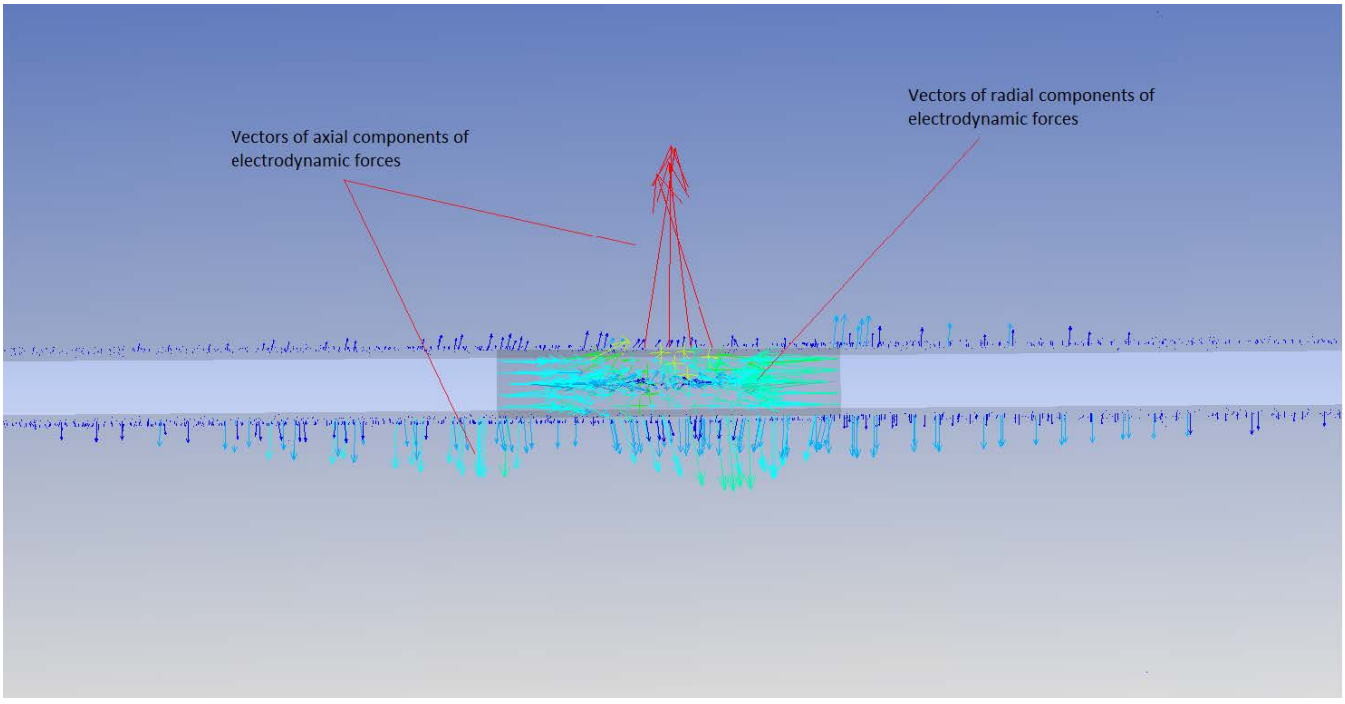

FIGURE 9. Components of electrodynamic forces in an analyzed contact system.

contact movement of the opposite sense. The reciprocal motion is magnified by the value of the generated electrodynamic forces.

The state without electrodynamic bounces usually occurs only after several bounces with decreasing amplitude and a shorter time of loss between the moving contact and the fixed contact.

Over the years, various methods have been developed to measure the duration of electrodynamic bounces. The simplest direct measurement of a single and total bounce time

is the recording of the voltage on a bouncing moving contact, from which the obtained data allow to draw a curve describing changes in the gap between the contacts while electrodynamic bounce occurs.

Another direct method is to use the laser beam as an optical probe to measure the length of the gap between the contacts placed between the light source (laser), the photosensor. In this case, the light source must be set so that the generated contact movement during electrodynamic bounces causes a change in the amount of light reaching the sensor. This method, however, requires optical access to the contacts and is not applicable in the case of an electric arc between the contacts.

Due to the above-mentioned difficulties, it is recommended to use indirect optical methods to measure electrodynamic bounces, including the method of recording light by a CCD (charge-coupled device) camera, which allows for the recording and then reading of an electrical signal proportional to the amount of incident light that lights on it. An example of a system for measuring electrodynamic springs of the method using a CCD camera is shown in the Figure 10 below.

It should be noted that it is not enough to register only the movement of the movable contact, because also the fixed contact is usually subject to elastic vibrations caused by the hitting of the movable contact against it.

Mechanical models for studying the phenomena of electrodynamic bounce as shown in Figure 11. Below.

Those can be used to study impact phenomena or to determine the coefficient of impact for a certain material.

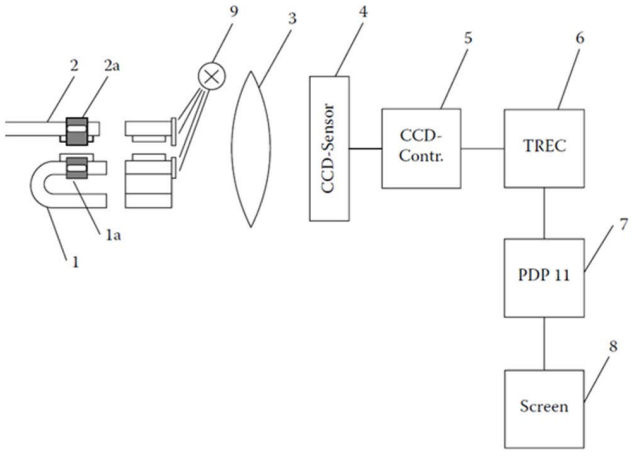

FIGURE 10. Recording of light reflected from contacts by CCD camera (1 - fixed contact; 2 - moving contact; 1a, 2a - contrast strips connected with contacts; 3 - lens; 4 - CCD sensor; 5 - CCD driver; 6 - transient recorder; 7 - computer; 8 - graphic screen; 9 - light source [5]).

In the designed contact, the clamping force value of the movable contact should be selected in such a way that in the case of the peak current of the connector, the spring pressure forces are greater than the expected electrodynamic force. In order to analyze the kinematic system that checks the time and amplitude of electrodynamic bounces, various contact models with specific degrees of contacts freedom are used,

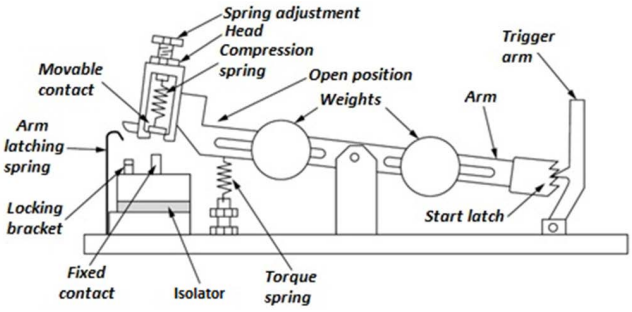

FIGURE 11. Shaw's contact bouncing control mechanism [5].

a model with two degrees of freedom will be reflected and will vibrate, causing bounces of smaller amplitude in turn, until those stop.

Due to the problematic effects of electrodynamic interactions in the form of bounces and electrodynamic repulsion force, various methods of limiting electrodynamic phenomena in contacts have been developed. These are among others listed below.

1. Setting the working surfaces of contacts at an angle an adynamic shaping shown in Figure 12:

$$F_e = F'_{ez} + F_{ek} \tag{4}$$

$$F'_{ez} = 2 \cdot F_{ez} \cdot cos\frac{\alpha}{2} \tag{5}$$

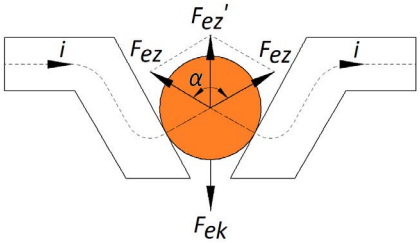

FIGURE 12. Setting the contact surfaces at an angle and electrodynamic compensation by means of adynamic shaping of the contact.

2. Contact sharing shown in Figure 13:

$$F_e = n \cdot F_{ez} \tag{6}$$

$$F_{ez} = k \cdot (1,3 \cdot \frac{i}{n})^2 \tag{7}$$

$$F_e = \frac{1,69}{n} \cdot k \cdot i^2 \tag{8}$$

$$F_e = 0,84 \cdot 5 \cdot k \cdot i^2 \text{ for } n = 2 \tag{9}$$

3. Electrodynamic compensation by dividing one contact into more parallel contacts (tulip contact) shown in Figure 14:

$$F_e = F_{ez} - \frac{F_{ek}}{2} \tag{10}$$

$$F_{ek} = 0,25 \cdot k_1 \cdot i^2 \cdot l \tag{11}$$

4. Compensation by shaping the current path in the form of a loop (single-loop, two-loop, multi-loop contacts)

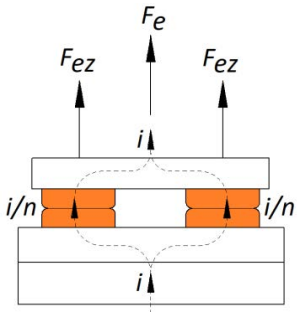

FIGURE 13. Sharing of a contact into several parallel contacts.

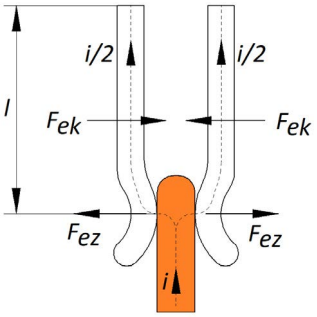

FIGURE 14. Electrodynamic compensation by splitting one contact into more parallel contacts (tulip contact system).

shown in Figure 15:

$$F_e = F_{ez} - F_{ek} \tag{12}$$

$$F_{ek} = k_1 \cdot i^2 \cdot l \tag{13}$$

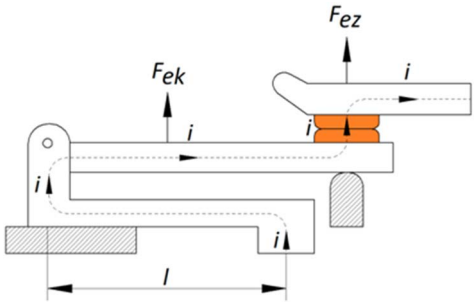

FIGURE 15. Compensation by shaping the current path in the form of a loop (single-loop, two-loop, multi-loop contacts).

5. Setting the working contact surfaces at an angle – for that scenario equations (4), (5) and (14) are employed. That was shown in Figure 16:

$$F'_{ez} < 2F_{ez} \tag{14}$$

In circuit-breakers with high current-carrying capacity of contacts, the system shown in Figure 16 is often used, in which the working surfaces of the contacts are set at an angle α in relation to the direction of interaction of the contact forces. In this case, the resultant force F'_{ez} is smaller than the sum of the electrodynamic forces F_{ez}, which is more

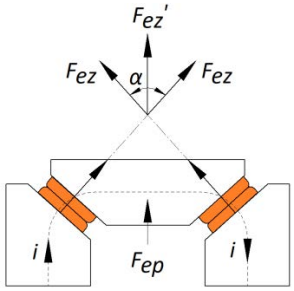

FIGURE 16. Setting the working contact surfaces at an angle.

favorable than in a typical contact. The circuit shown in Figure 12 has additional, more advantageous features due to the adynamic shape of the contact allowing for additional electrodynamic compensation of the forces that push the contacts away from each other. For contactors and circuit breakers, the example shown in Figure 13 is used, which is employed to separate the flowing current by using several parallel contacts. In this case, the arising electrodynamic forces in the contact have smaller values because the current value in a given contact is lower. Example shown in Figure 16 is found in medium voltage circuit breakers which are equipped with tulip contacts. Evenly spaced contacts are pressed against the pin by compression springs. In this case, during the flow of rated or short-circuit currents, the contact pressure force through the pressure springs is increased by the additional action of electrodynamic forces F_{ek} compensating the electrodynamic forces F_{ez} acting at the contact point of the contact system.

The above-mentioned theoretical methods of the compensation of electrodynamic forces in the contacts of electric devices were used by the authors in order to perform simulation calculations to verify the presented methods.

For this purpose, a 3D model presenting the geometry of the system 5 (Figure 16) was made, where the working surfaces of the contacts were positioned at an angle α in relation to the direction of interaction of contact forces, in accordance with the theoretical assumptions. After importing the model to the software, the boundary conditions were assigned and a simulation for a short-circuit current of 40 kA was performed.

After the computational simulation was performed, the current density distribution in the analyzed contact system was derived. The highest values of the short-circuit current density were found at the contact points, as shown in Figure 17 below.

The determined values of the electrodynamic forces in the executed simulation reached the average of 10 – 40 $\boldsymbol{N/m^3}$. The maximum value achieved was witnessed in the right contact of the current path shown and it amounted to 50 $\boldsymbol{N/m^3}$. This was shown in Figure 18 below.

The performed calculations confirmed the presented return of the electrodynamic forces $\boldsymbol{F_{ez}}$ acting in the contact, which at the same time confirms the thesis that the angular arrangement of the contacts allows for the reduction of the

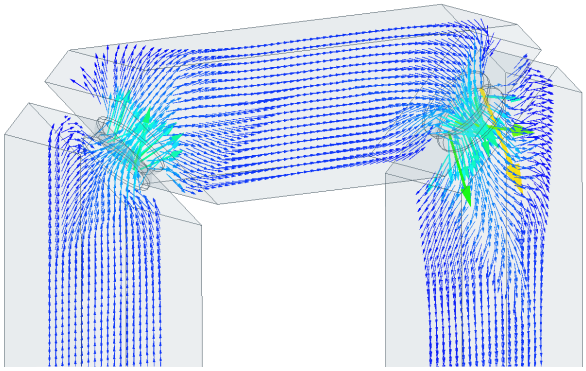

FIGURE 17. Current density distribution in the system compensating the effect of electrodynamic forces—arrangement of the contacts at an angle.

electrodynamic forces value that ought to open the analyzed contact. Force F'_{ez} value was smaller than force F_{ez} value. It is worth noting that the highest stresses in the computational simulation performed occurred in the center of the contact strips, where the radial component of the generated electrodynamic forces was revealed, causing the contact material to compress at the point of actual contact of. The stress distribution in the analyzed contact system is presented in Figure 19 below.

V. ELECTRODYNAMIC FORCES IN CLASSIC TULIP CONTACT LAYOUT

Analyzing furtherly the theoretical assumptions concerning the compensation of electrodynamic interactions in contacts, a 3D model of a tulip contact with specially elongated contacts of the contact crown was prepared. In this case, the generated force pressing the tulip lamellas against the arcing contact and the forces pushing the contacts at the point of contact with the pin were analyzed. In order to determine the interaction of electrodynamic forces in the tulip contact, a short-circuit current of 40 kA was passed through the contact along with the non-periodic component of the current raising it to 50 kA in the initial phase of its duration. The obtained waveform is shown below in Figure 20. The voltage level value for those simulations was set at 72,5 kV. For this voltage, the device can be filled with CO_2 or SF_6 gas. Of course, the extinguishing medium determines the current carrying capacity. And so for CO_2 gas this load capacity is, for example, 2750 A, and for the same cross-sections when filled with SF6 gas it is equal to 4000 A. Undoubtedly, it is related to the ability to receive energy from the electric arc and deionizing the contact gap. The key decision related to the selection of the contact system for research and analysis was the trend:

- restrictions on the use of SF_6 gas,
- developing the process and mechanism of thermal exposure to the next generations,
- research on the use of CO_2 gas and its mixtures and also other gases.

Current flowing through the tulip contact was analyzed, the highest current density was demonstrated at the contact points between the lamellas and the contact pin inserted into the crown formed by the system. Additionally, the distribution of the short-circuit current density flowing through the contact is presented in the Figure 21 above.

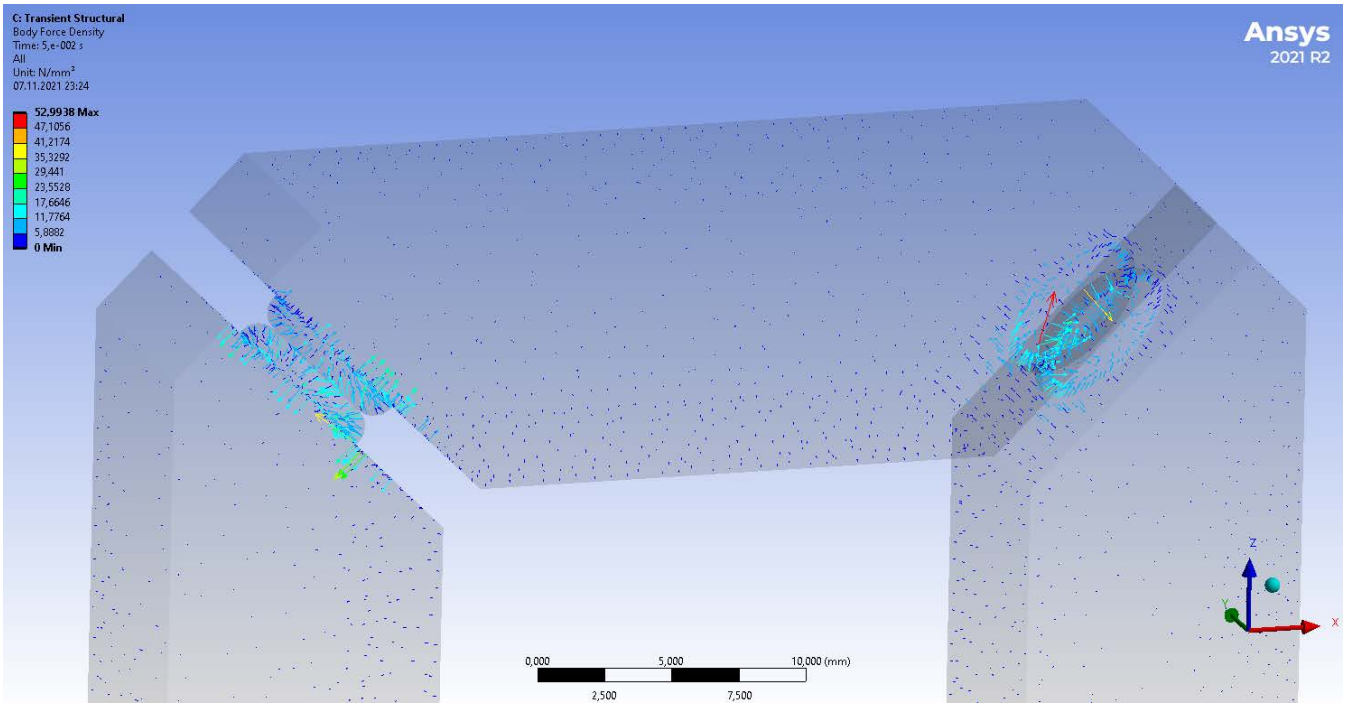

FIGURE 18. Distribution of electrodynamic forces in a contact - arrangement of contacts at an angle.

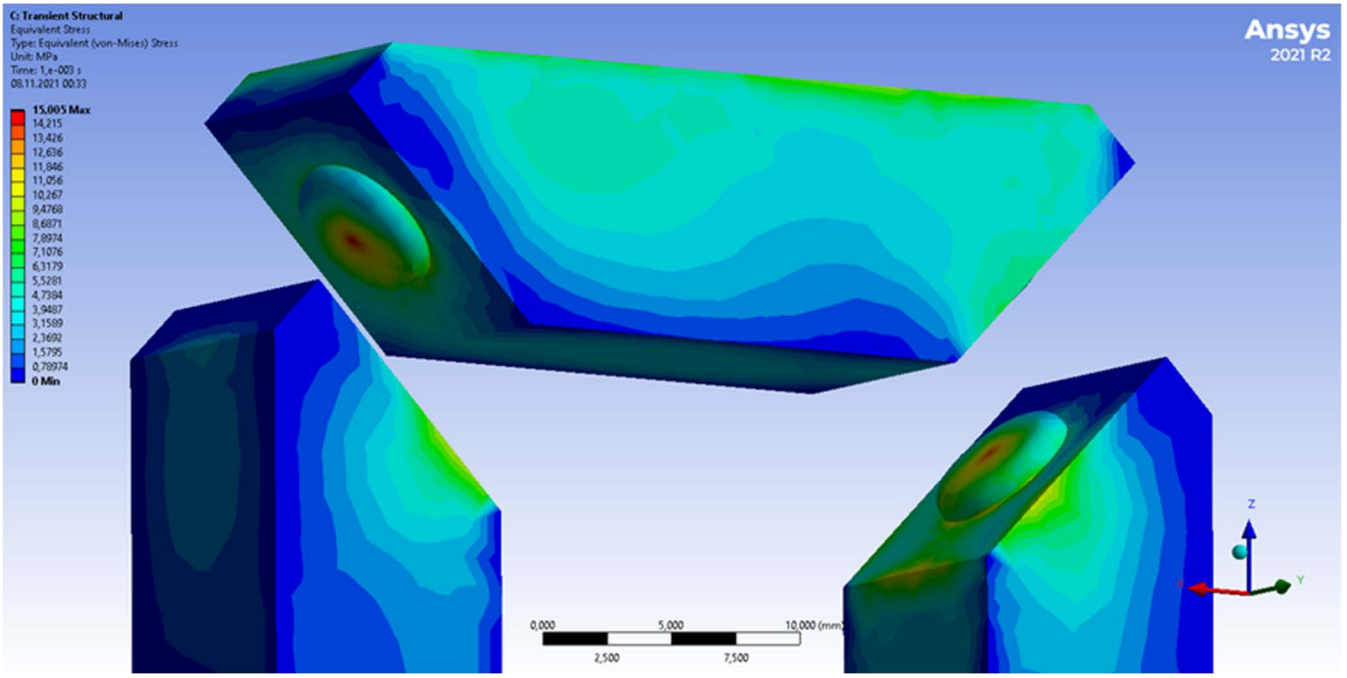

FIGURE 19. Distribution of electrodynamic forces in a contact - arrangement of contacts at an angle.

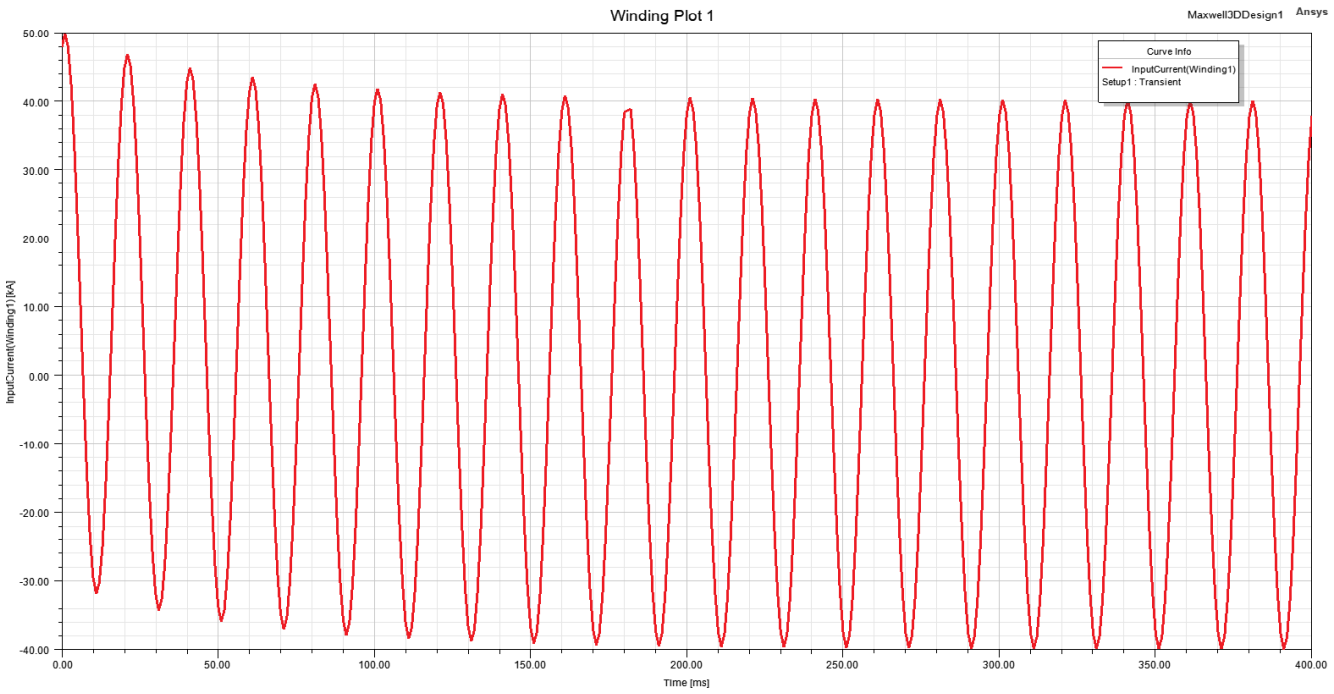

FIGURE 20. Generated simulation of the short-circuit current passed through the analyzed tulip contact.

After exporting the obtained computational data to the mechanical solver, it was possible to generate the distribution of the resulting electrodynamic forces in the analyzed tulip contact. In this case, the theoretical assumptions were confirmed, where forces $\boldsymbol{F_{ez}}$ were generated at the contact points, repelling the contacts of the contact crown from the contact pin. In the remaining parts of the contactor, electrodynamic forces $\boldsymbol{F_{ek}}$ were created, pressing all the contacts inwards, thus eliminating the impact of the forces repulsing the lamellas. The generated electrodynamic force vectors are shown below in the Figure 22 above.

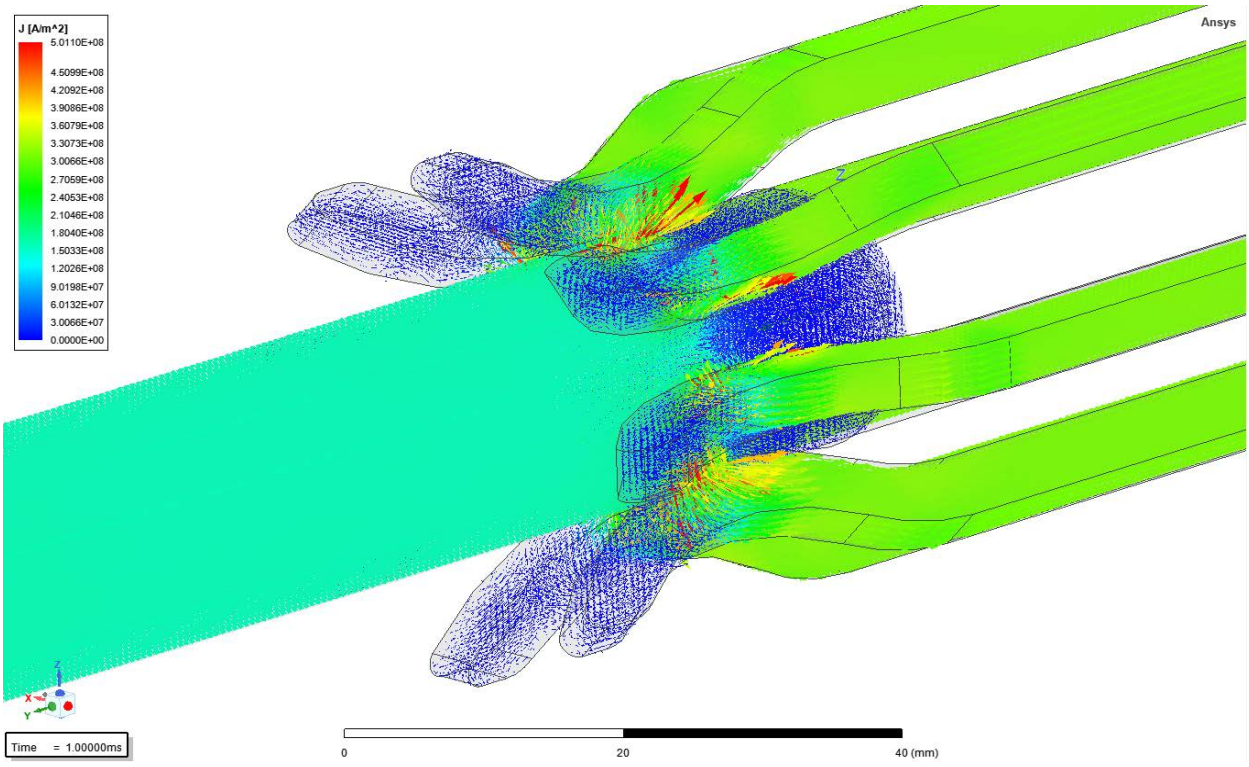

FIGURE 21. Short-circuit current density flowing through the tulip contact.

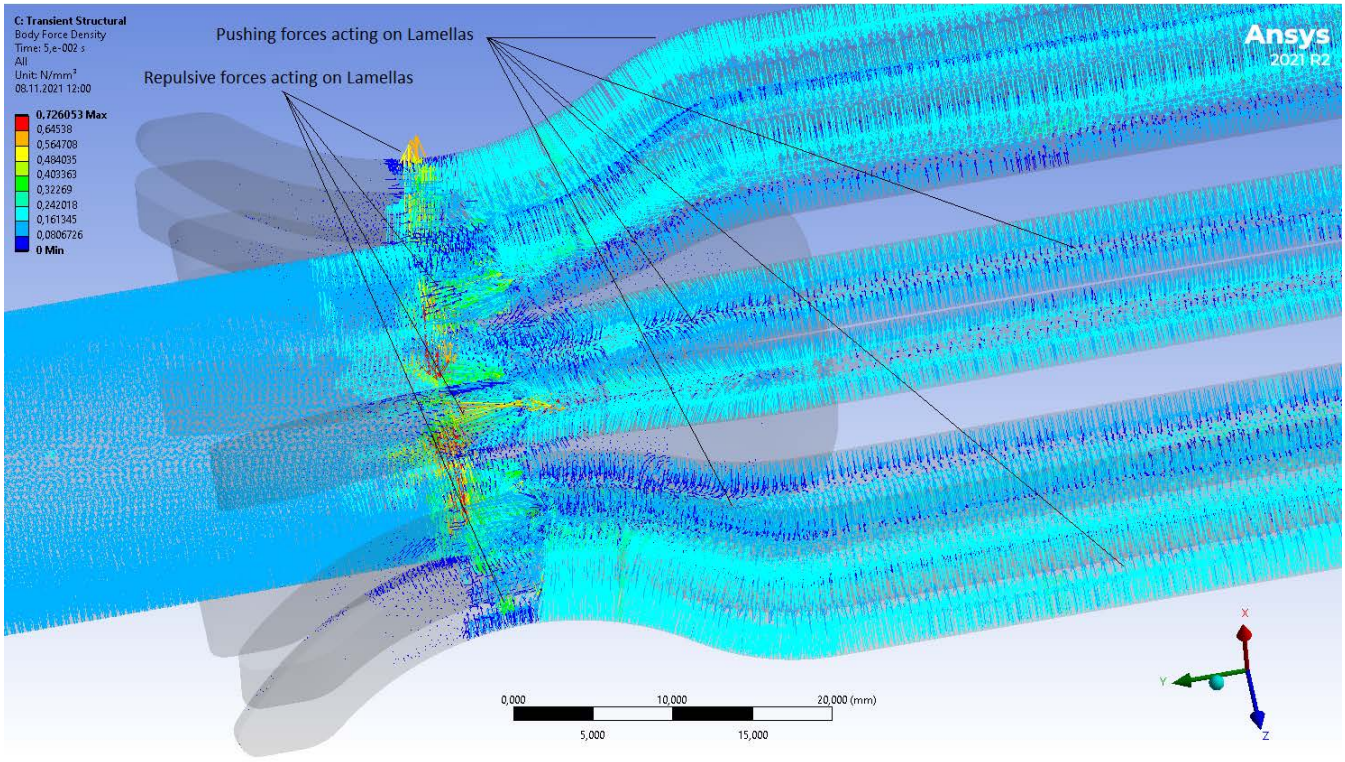

FIGURE 22. Distribution of the interacting electrodynamic forces at the actual contact points and the entire tulip contact body.

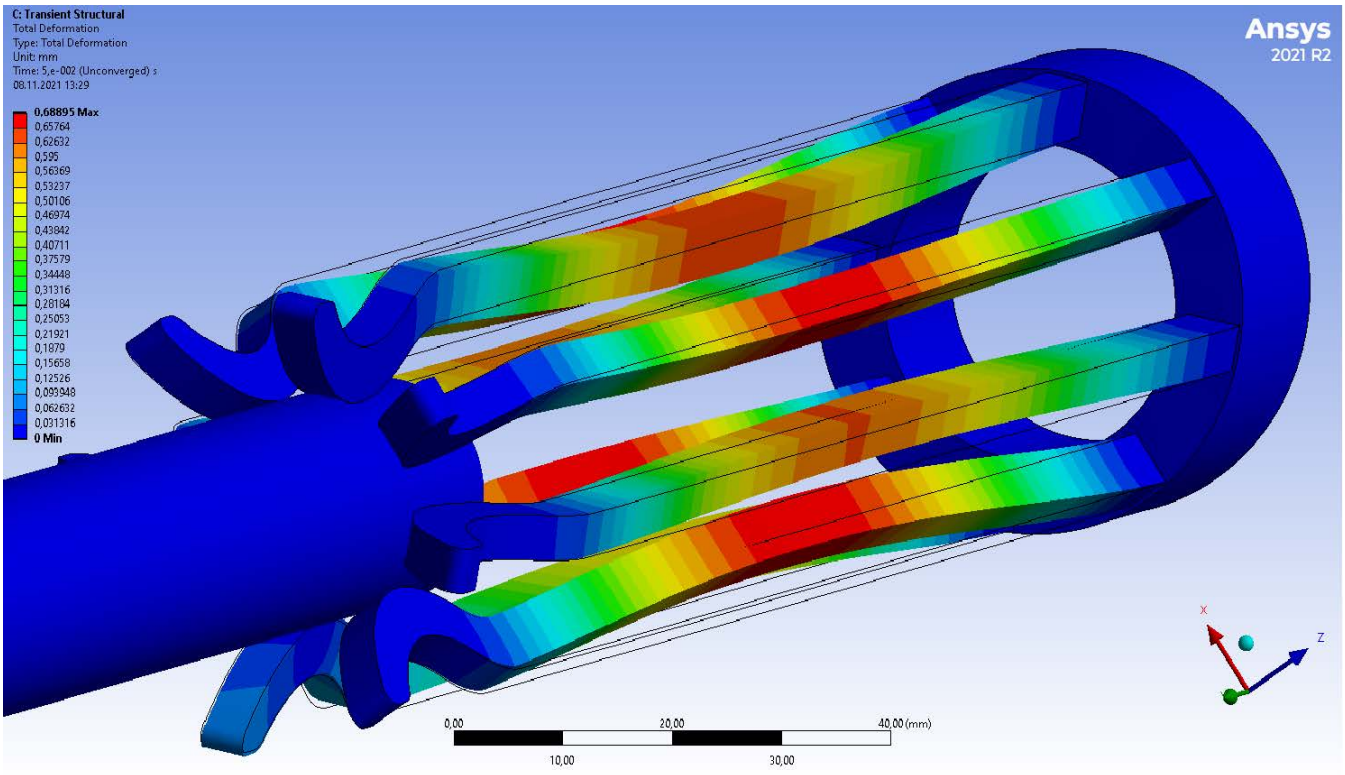

FIGURE 23. Contact mechanical deformations in a tulip contact related to the interaction of electrodynamic forces.

In order to verify which electrodynamic forces are greater, an additional mechanical analysis was performed to check where the greatest mechanical deformations occur. In the computational simulation, it turned out that the electrodynamic forces at the point of contact have a much lower value than the forces pressing the contactors. This is illustrated in detail in Figure 23 above, where the deformations related to the occurrence of the discussed forces in the tulip contact are presented.

VI. ELECTRODYNAMIC FORCES IN HIGH VOLTAGE APPARATUSSES–LIVE TANK CIRCUIT BREAKER

High voltage electrical apparatuses such as circuit breakers and disconnectors are connected in series to the protected circuit. When disturbances in the form of short-circuits occur, the flowing short-circuit currents can be greater multiple times than the rated currents of these devices. In effect, generation of mechanical stresses is a result of electrodynamic interactions.

Manufacturers of alike devices can successfully use modern numerical methods in order to design and manufacture apparatuses resistant to the impact of electrodynamic forces. Simulation analyses allow to determine the value of electrodynamic forces originating from peak short-circuit currents and mechanical stresses resulting in the developed layouts of high voltage electrical apparatuses. The electrodynamic force of the designed device is defined by the peak value of the current switched off, for example, by a high-voltage switch without depriving it of its ability to be used further (it is not causing its damage).

One of the most important high voltage apparatuses are circuit breakers. Those allow for switching off fault currents, e.g. short-circuit currents in a protected circuit after receiving a signal from the protection automatics in order to start the circuit breaker drive. An example of the design of a circuit-breaker with three poles mounted on a common supporting beam with a common operating mechanism is shown below in Figure 24.

Development of the structure and production of a high-voltage circuit breaker requires from the manufacturer not only constructional knowledge and ''know-how'', but also a large technical base and machinery park. Global manufacturers such as ABB, SIEMENS or ALSTOM produce overhead circuit breakers for voltages up to 300 kV and for currents up to 50 kA in a single-break version, i.e. with one set of connection chambers for a particular pole of the HV switch. In the case of higher voltages, systems with a double set of switching chambers (420 kV) and with a four set of switching chambers (800 kV) are used.

There are two typical designs of SF_6 gas overhead switches in the circuit breaker design. The first type are the live-tank circuit breakers, the connection chamber of which is built into a porcelain or composite insulator at high potential

FIGURE 24. LTB-D high voltage Live-Tank circuit breaker by ABB.

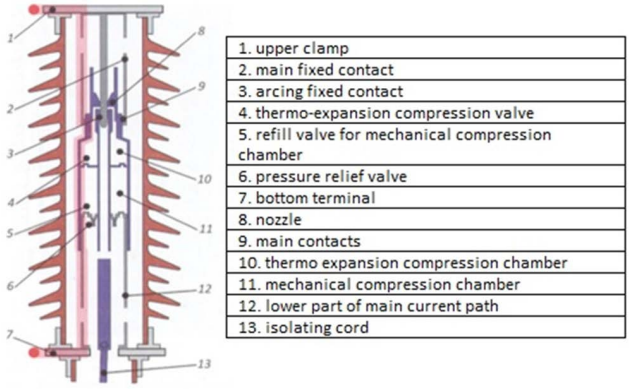

FIGURE 25. Longitudinal section of the HV circuit breaker connection chamber with SF_6 - third generation thermo-expansion.

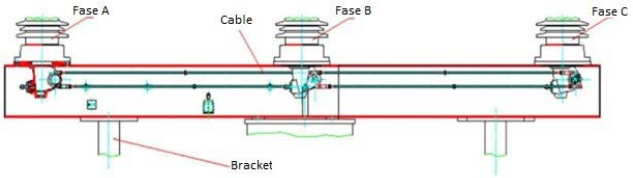

FIGURE 26. Schematic drawing of cables connecting the mechanisms of HV switch for 3 poles.

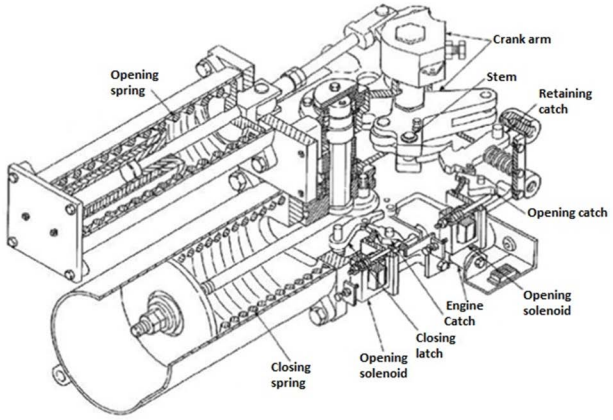

FIGURE 27. The pictorial drawing of a common drive for HV storage circuit breaker.

during operation. The second type of switches are dead-tank constructions, the tank of which, together with the connection chamber, works at the ground potential.

In this type of SF_6 circuit-breakers, the switching chambers are equipped with a puffer type, in which the gas is compressed by a piston or a cylinder directly coupled with the contact system. In the third generation of switches in the switching chambers, the thermal expansion effect is additionally used. The energy generated by the burning of the electric arc helps to extinguish it. During the opening or closing operation of the switch, the gas is compressed by a piston moving in a cylinder. The forced SF_6 gas into the extinguishing chamber flows around and cools the burning electric arc.

Currently used high-voltage circuit breakers are equipped with two-stream structures of extinguishing chambers, where SF_6 gas from the compression chamber is forced into a double system of nozzles with arcing contacts made of the main and auxiliary nozzles. Development work on the use of electric arc energy to increase the arc extinguishing efficiency during the zero crossing of the current, enabled the development of compression chambers consisting of two smaller chambers: thermal-expansion compression and mechanical compression. An example of the compression chambers built into the circuit breaker switching chamber is presented below in Figure 25.

The arcing contacts built into the switching chamber are most exposed to the effects of an electric arc during switching operations. The arcing contact system and the main contact system in the switching chamber operate in a specific switching sequence. When switching off e.g. fault currents, first the main contact of the switch opens without arcing, and then the arcing contact opens, taking over the erosive processes related to the action of the electric arc for which it is adapted (made of an alloy of tungsten or molybdenum with copper). When closing the circuit-breaker, the arc sequence of the arcing contact and the main contact are reversed.

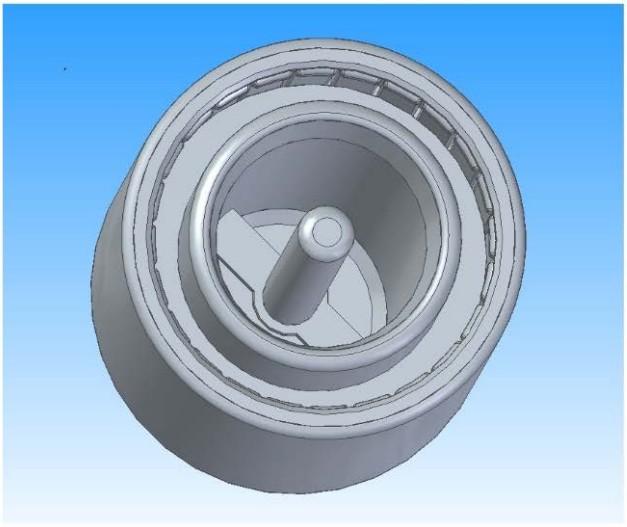

FIGURE 28. Modeled 3D assembly of the HV switch according to the executed measurements.

VII. LIVE TANK CIRCUIT BREAKER 3D MODEL AND ELECTRODYNAMIC FORCES SIMULATIONS

To create a 3D simulation model of a live tank high voltage circuit breaker, the dimensions were taken from a real object. From the outside, the switch pole was made of a supporting insulator to which the extinguishing chamber of a single-break switch is screwed. The circuit-breaker has connections for screwing high-voltage cables and screw fittings for mounting the pole on the support beam of the three-pole system. Inside the circuit breaker, at the height of the supporting insulator, there is a string coupled with a piston moving inside the cylinder in the connection chamber. The traction layer is mechanically stressed with the mechanism of the entire circuit breaker. The power from the drive is transferred by means of strings to individual poles, where the contacts of the switch are closed or opened. An illustrative drawing of the mechanical system of the traction layers is presented in Figure 26 below. The traction layers are driven from the switch storage drive located under the middle pole of the switch (phase B). The energy from the closing and opening springs is transferred to the circuit-breaker poles by means of the strings. The main components of the storage drive of the high-voltage circuit breaker are described in Figure 27 below.

In the switching chamber, on the moving piston, there is a movable part of the arcing contact in the form of six lamellas and a movable part of the main contact of the analyzed circuit breaker (sleeve). The fixed elements of the arcing contact and the main switch, due to the fact that the circuit breaker was of the single-motion type, are the main crown with the main contact contacts and the arcing contact in the form of a bar overlapping the crown.

The circuit breaker components have been accurately measured and dimensioned. This allowed for the preparation of 3D models of individual elements of the high-voltage circuit breaker connection chamber, including: main contacts, arcing contact, nozzle, cylinder and other elements. The prepared 3D assembly of modeled elements of the high-voltage switch structure is shown in Figure 28 above and in

The 3D modeled simplified structure of the high-voltage circuit breaker chamber made it possible to perform simulation analyses of electrodynamic forces for the short-circuit

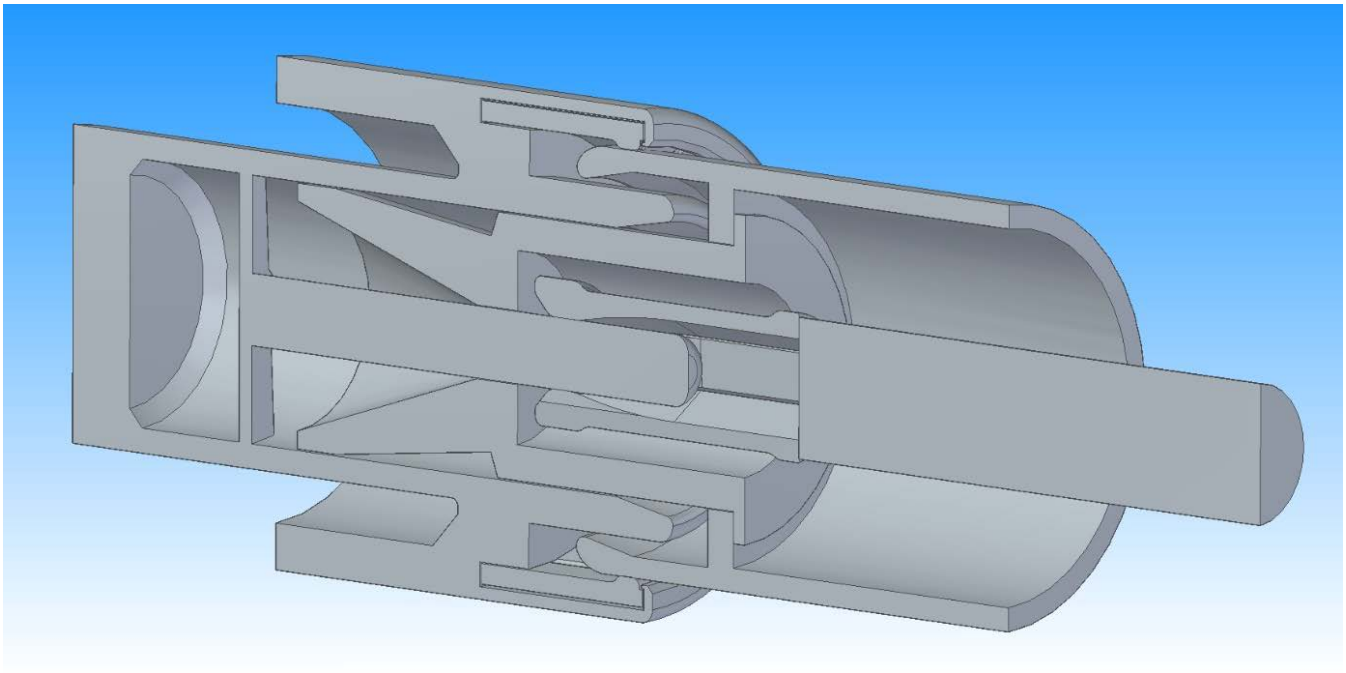

FIGURE 29. Modeled 3D assembly of the HV switch according to the executed measurements—cross section.

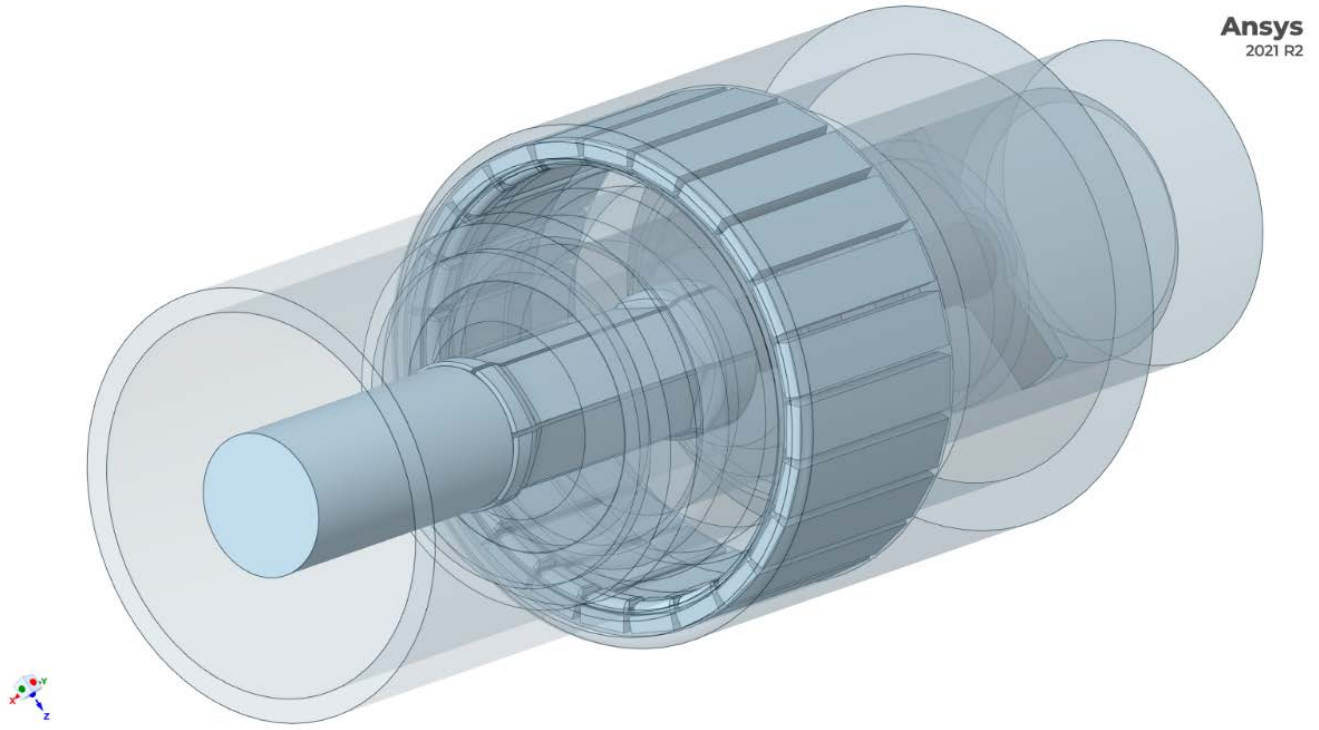

FIGURE 30. Optimized geometry of HV breaker in Ansys space claim module.

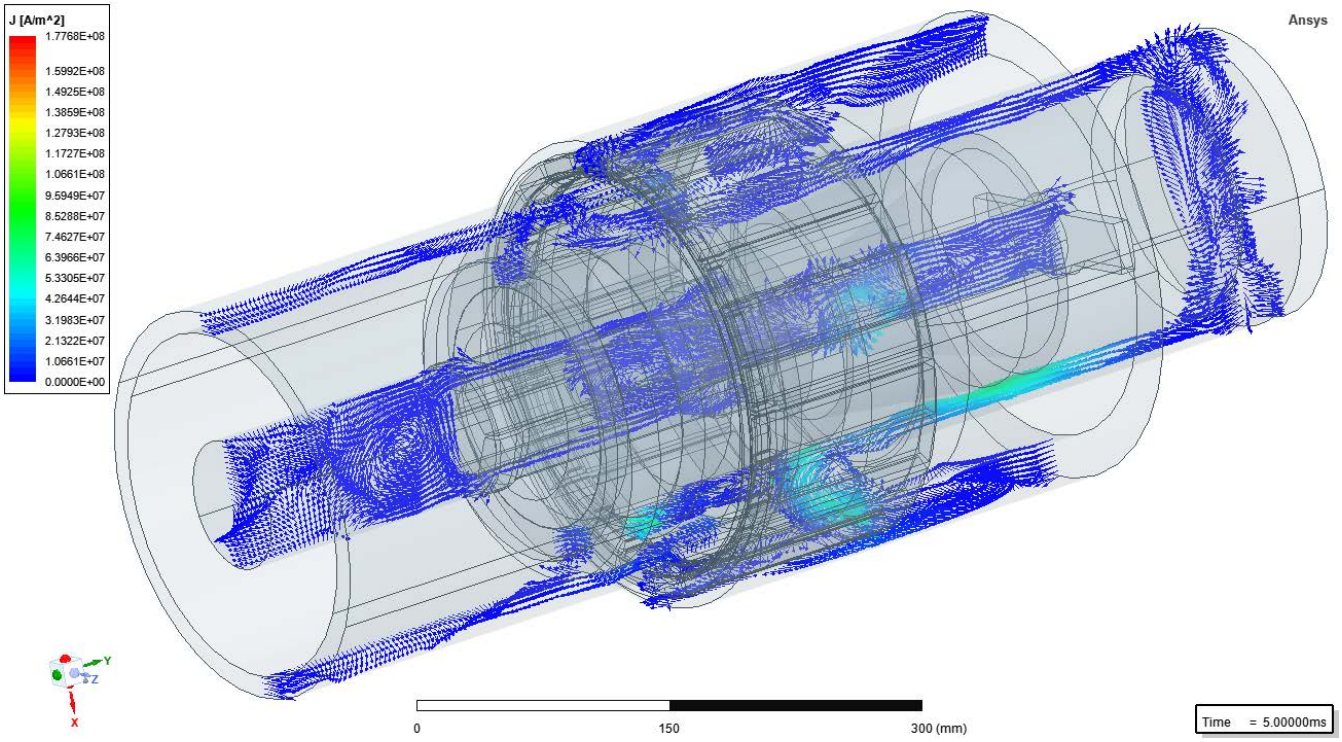

FIGURE 31. Density distribution of the short-circuit current flowing through the contacts of the switching chamber of the high-voltage circuit breaker.

conditions declared by the manufacturer in the form of 40 kA of rated short-circuit breaking current.

For this purpose, the prepared 3D model of the circuit breaker connection chamber was imported into the Ansys

Workbench software, where in the Space Claim Geometry module, the geometry was thoroughly checked and simplified in terms of the quality of modeled parts - redundant surfaces and duplicated unnecessary edges. The geometry was prepared in this way, devoid of any non-linearities and inaccuracies causing problems during calculations. It was shown in Figure 30 above.

In order to prepare a computational simulation, the 3D model was exported to the Ansys Maxwell 3D computational module. The simulation analysis to determine the electrodynamic forces in the contacts of the circuit breaker at the moment of the short-circuit current occurrence was performed for the closed main and arcing contacts of the circuit breaker. The imported 3D model of the circuit breaker into the Ansys Maxwell 3D environment was properly prepared for simulation. For the calculations, environmental conditions in the form of SF_6 gas were adopted and material properties were assigned to individual parts of the analyzed assembly of the HV switch. Examples of material properties for tungsten adopted for the arcing contact pin are shown in the Table 1 below.

After setting the material properties, the model was given current forces in the form of specific short-circuit currents. The initial direction of current flow for calculations was assumed from the fixed contacts to the moving contacts of the circuit breaker. Simulation analyses to determine the value of electrodynamic interactions in the circuit breaker contacts were performed for two cases of short-circuit current:

- 40 kA without non-periodic component,
- 40 kA with a non-periodic component increasing the short-circuit current up to 60 kA.

Boundary conditions for the prepared simulation were properly determined, it was necessary to determine the simulation time, the duration of which was assumed to be 200 ms. The time step for the computational iterations performed was assumed every 0.5 ms, which gave a total of 400 iteration steps that the solver had to perform.

In the case of the ''mesh'' calculation, elements of the ''tetrahedra'' type were used. On the contact points of the crown of the main contact and the arcing contact, the computational grid was additionally densified in order to obtain greater accuracy of calculations. In the first computational iteration, the number of mesh elements was 534379, the ''Adaptive Mesh Refinement'' function was employed, the mesh was compacted by a solver in places where it was additionally required.

Numerical calculations were started, the total time of which was 10.5 hours. From the obtained results, it was possible to check which elements of the switching chamber are most exposed to electrodynamic influences generated by the flow of short-circuit currents. At this stage of the calculations, it was also possible to analyze the generated approximate Ohm losses in each of the analyzed active parts of the circuit breaker. Additionally, the software made it possible to view the density distribution of the short-circuit current flowing through the closed contacts of the high-voltage switch, an example of the density distribution in the contact system is shown below in Figure 31. In the case of the simulation analysis performed, particular attention was paid to the forces occurring in the contacts of the main and arcing contacts.

For the first numerical simulation, for an undistorted short-circuit current of 40 kA, the values of electrodynamic forces in the main contact were similar to the order of magnitude for all 24 main contactors (lamellas) (force values in kN). However, the calculated values of electrodynamic forces for

TABLE 1. Examples of material properties for tungsten used for calculations in the simulation analysis for the switching chamber of the high-voltage circuit breaker.

Name	Type	Value	Units
Relative Permittivity	Simple	1	
Relative Permeability	Simple	1	
Bulk Conductivity	Simple	$182 \cdot 10^5$	siemens/m
Dielectric Loss Tangent	Simple	0	
Magnetic Loss Tangent	Simple	0	
Electric Coercivity	Vector		
Magnitude	Vector Mag	0	
Magnetic Coercivity	Vector		
Magnitude	Vector Mag	0	A per meter
Thermal Conductivity	Simple	174	W/m·C
Magnetic Saturation	Simple	0	tesla
Lande G Factor	Simple	2	
Delta H	Simple	0	A per meter
Measured Frequency	Simple	9.4e+09	Hz
Core Loss Model		None	w/m^3
Mass Density	Simple	19300	kg/m^3
Composition		Solid	
Specific Heat	Simple	132	j/kg·C
Young's Modulus	Simple	$375 \cdot 10^9$	N/m^2
Positions Ratio	Simple	0.3	
Thermal Expansion Coefficient	Simple	4.6e·06	1/C
Magnetostriction	Custom		
Inverse Magnetostriction	Custom		
Thermal Material Type		Solid	
Solar Behavior	Simple	0	

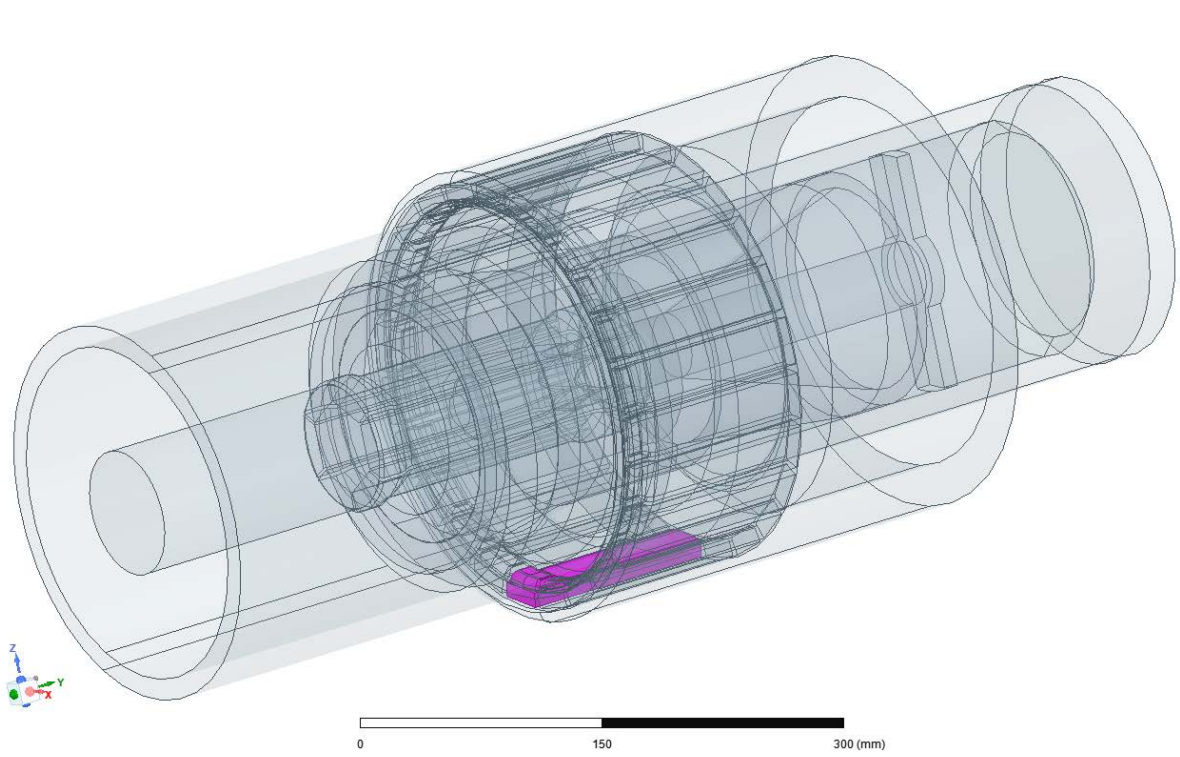

FIGURE 32. 1 of 24 lamellas (contactors) of the main contact in high voltage circuit breaker before simulation.

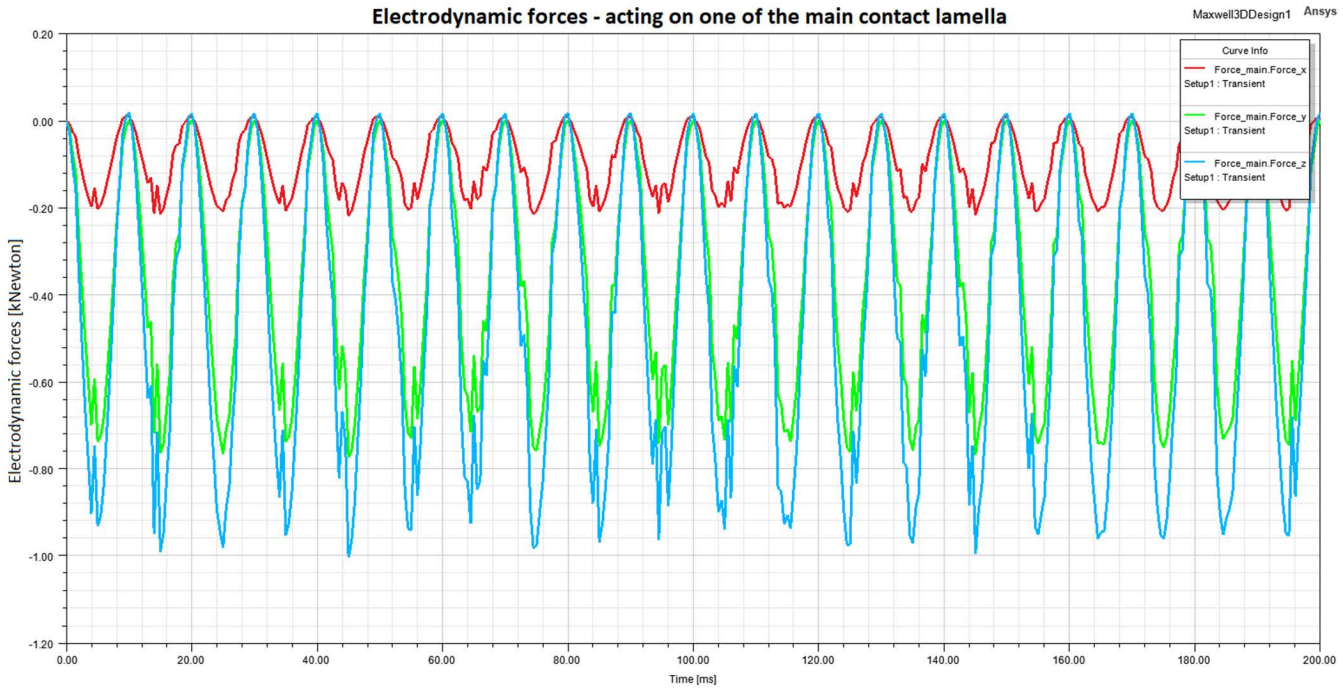

FIGURE 33. Values of electrodynamic forces acting on one of the main contact lamella for 40 kA without non-periodic component.

the contact points were different and ranged from 0.01 to 1.2 kN. An example of the generated electrodynamic forces for 1 of the 24 main lamellas is presented in Figure 32 above and Figure 33 below.

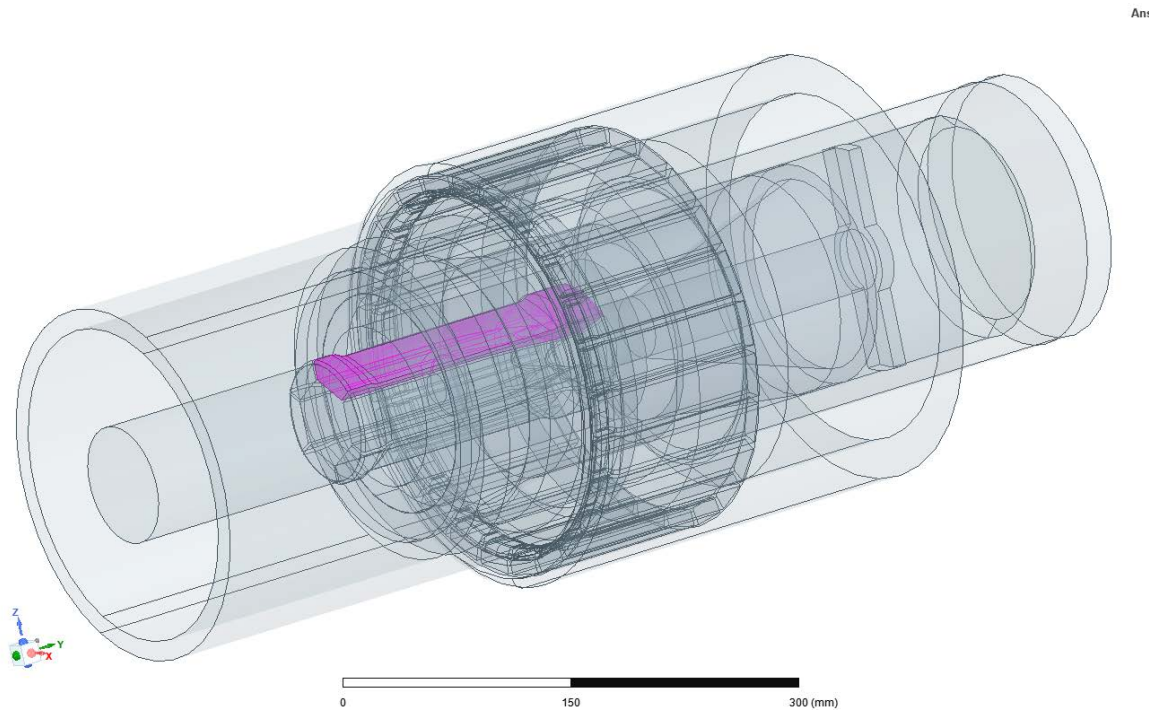

FIGURE 34. 1 of 6 lamellas (contactors) of the arcing contact in high voltage circuit breaker before simulation.

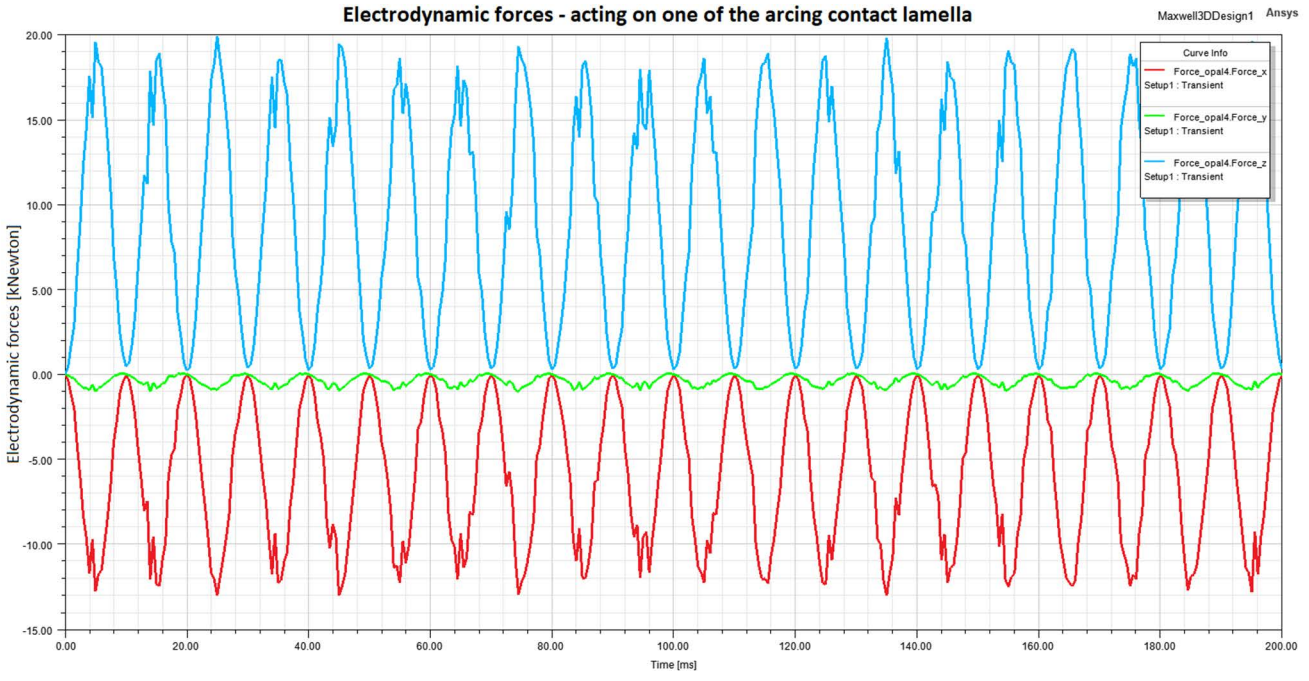

FIGURE 35. Values of electrodynamic forces acting on one of the arcing contact lamella for 40 kA without non-periodic component.

In Figures 34 above and Figure 35 below the simulation for 1 of 6 lamellas of the arcing contact were depicted for the 40 kA current without non-periodic component.

The results of the second computational simulation for the current with a non-periodic component shown that contacts were under influence of significant electrodynamic loads. It was dependent on the presence of a non-periodic component boosting the short-circuit current in the initial phase of its duration. The momentary boost of the short-circuit current value resulted in higher electrodynamic loads in the

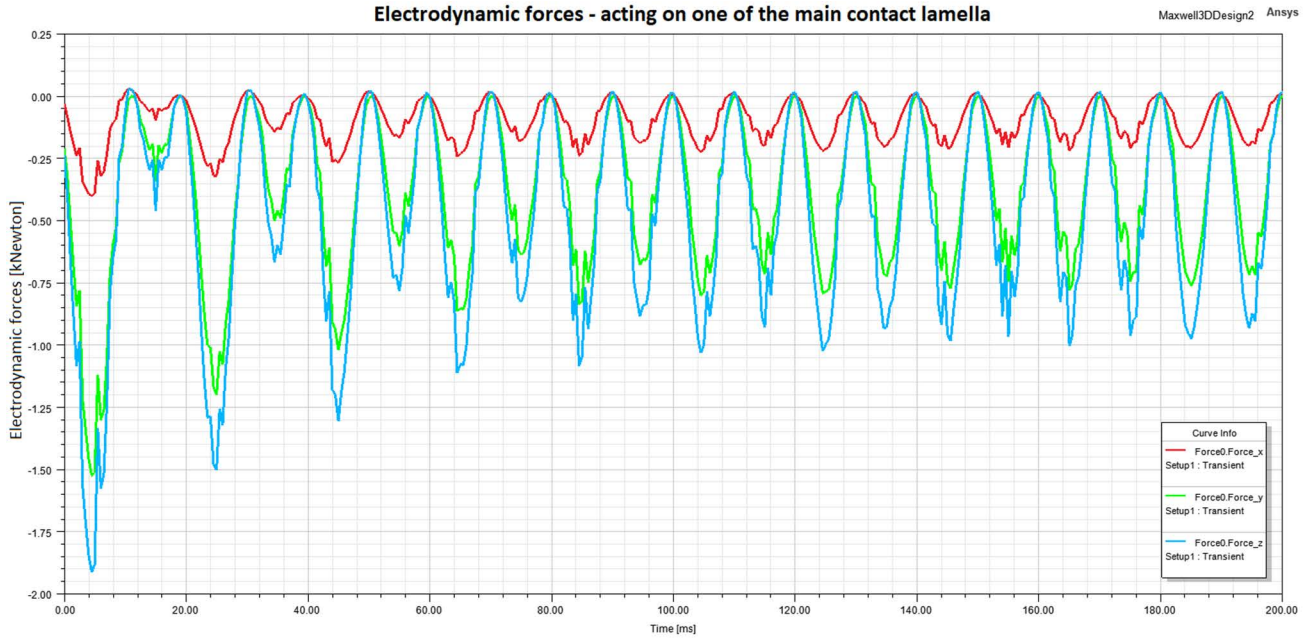

FIGURE 36. Values of electrodynamic forces acting on one of the main contact lamella for 40 kA with a non-periodic component increasing the short-circuit current up to 60 kA.

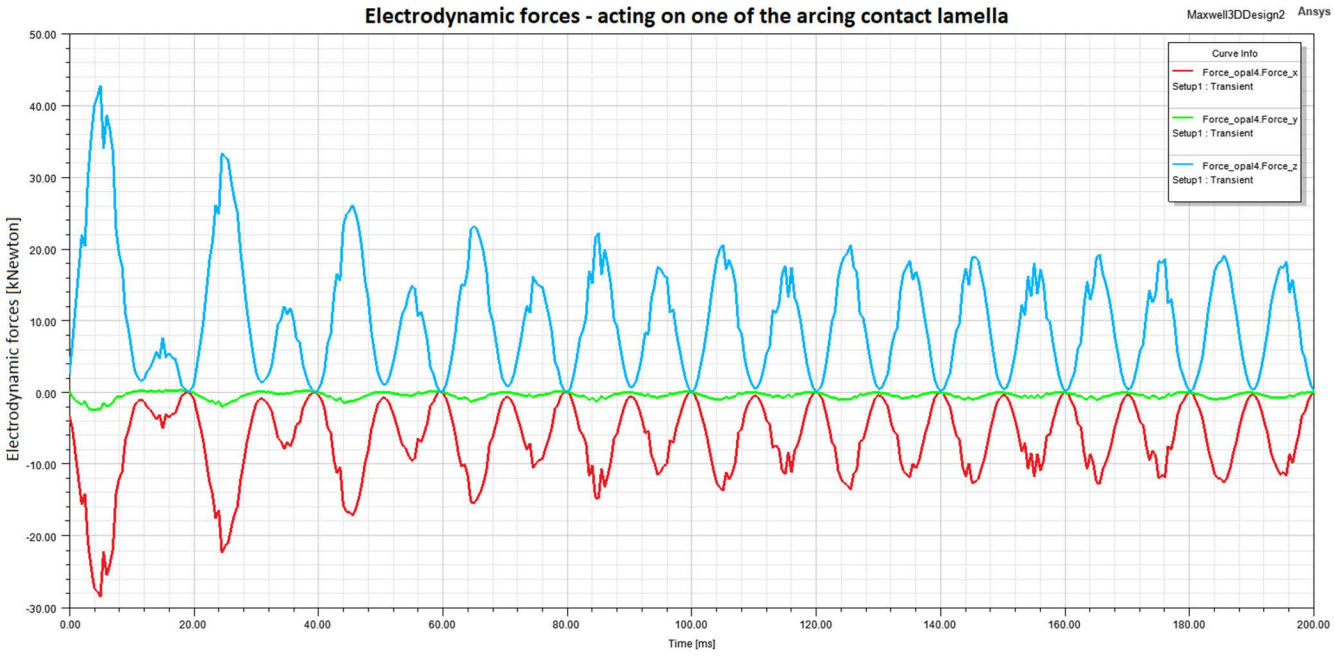

FIGURE 37. Values of electrodynamic forces acting on one of the arcing contact lamella for 40 kA with a non-periodic component increasing the short-circuit current up to 60 kA.

circuit breaker contacts. In the case of the main contact, the maximum value of the electrodynamic forces reached twice the value of about 2.5 kN, and then at the time of the decay of the non-periodic component, these values decreased to the level of the results from the previous calculations. Sample waveforms for a selected contactor are shown in Figure 36 below.

The electrodynamic effects for 40 kA current with a non-periodic component in the arcing contact are much greater. In relation to the simulation results for the arcing contact loaded with a current without a non-periodic component the calculated values are twice as high, reaching over 40 N. The values for the selected arcing contactor are shown in Figure 37 below.

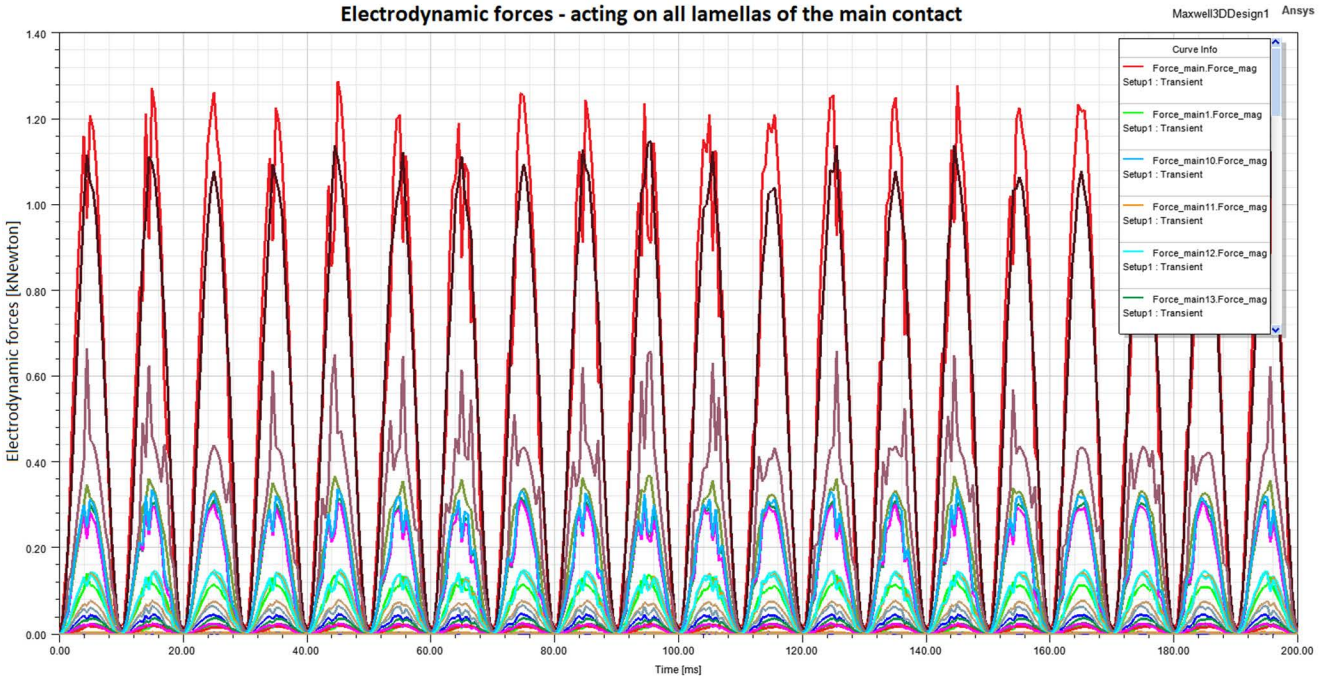

FIGURE 38. Values of electrodynamic forces acting on all lamellas of the arcing contact of the Live Tank high-voltage circuit breaker for short-circuit current without non-periodic component—arcing contact.

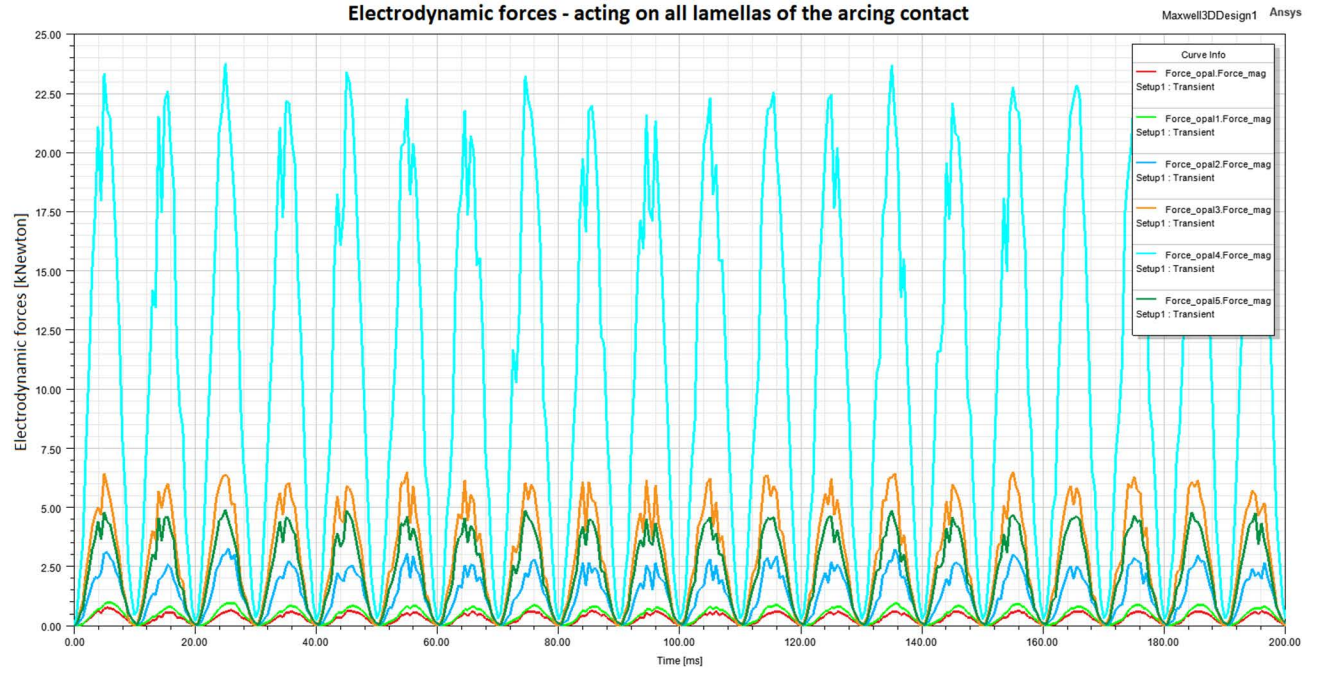

FIGURE 39. Values of electrodynamic forces acting on all lamellas of the main contact of the Live Tank high-voltage circuit breaker for short-circuit current without non-periodic component—main contact.

The obtained values illustrate the formation of momentary significant increases in electrodynamic interactions in the initial phase of the current flow in relation to the previous calculations for the short-circuit current without the non-periodic component.

The use of the 3D model of the circuit breaker switching chamber made it possible to perform very time-consuming calculations aimed at determining the electrodynamic interactions on all contacts. This unique approach made it possible to verify that all contacts in the contact system are evenly

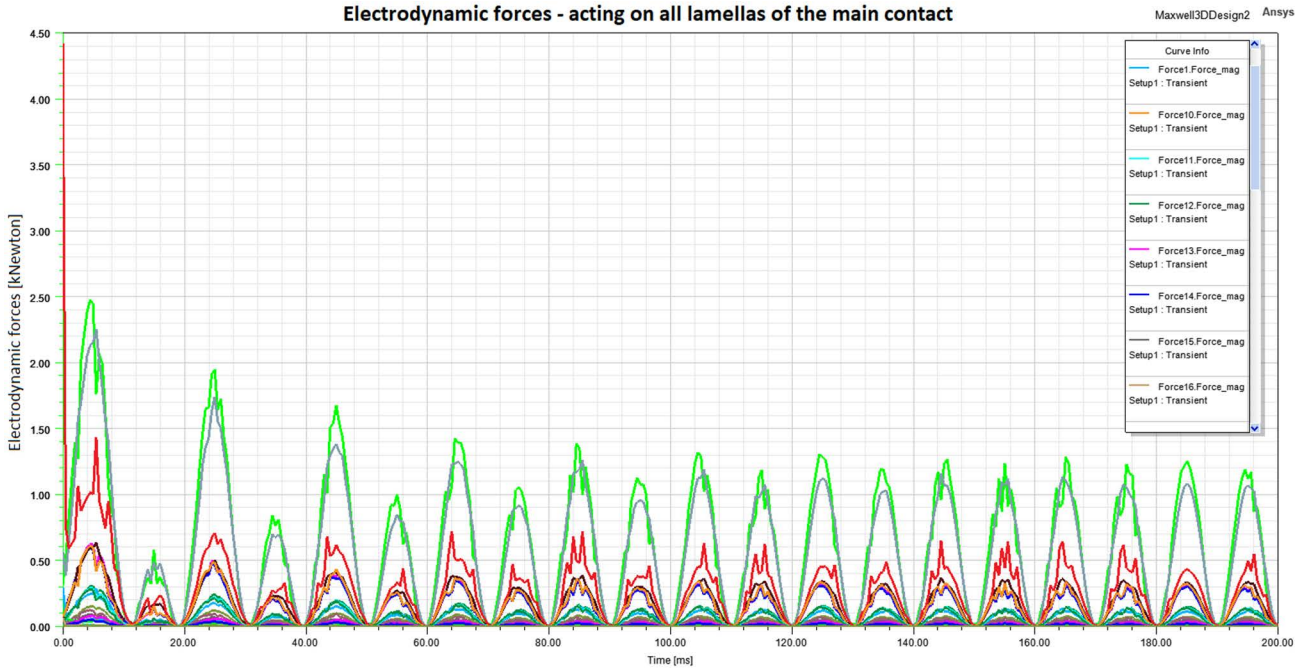

FIGURE 40. Values of electrodynamic forces acting on all lamellas of the main contact of the Live Tank high-voltage circuit breaker for short-circuit current with non-periodic component—arcing contact.

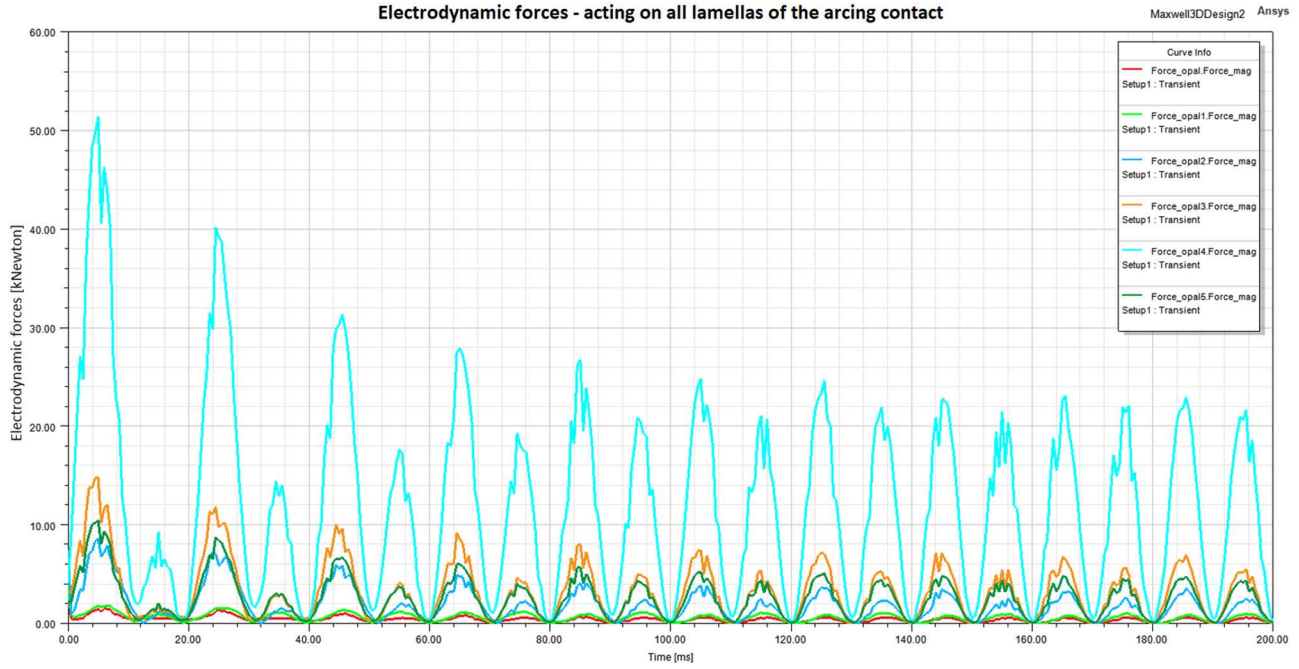

FIGURE 41. Values of electrodynamic forces acting on all lamellas of the main contact of the Live Tank high-voltage circuit breaker for short-circuit current with non-periodic component—arcing contact.

loaded. Calculations were executed for 1.265.243 generated computing nodes. As a result, it was possible to generate the resultant waveforms of electrodynamic interactions affecting the main and arcing contacts. It was presented in Figures 38-41 below.

VIII. SIMULATION RESULTS SUMMARY

The generated waveforms allowed for the analysis and conclusions that the main and arcing contacts are not uniformly electrodynamically loaded during a 40 kA short-circuit with a course not deformed by a non-periodic component. The same

computational approach was performed for the short-circuit current much more unfavorably from the point of view of electrodynamic exposures, which contains a non-periodic component. This type of short-circuit current is much more harmful from the point of view of mechanical stresses - deformation or even contact damage. The calculations made in the form of generated waveforms for the main and arcing contact contacts for a more unfavorable short-circuit current were collected on the waveforms depicted in Figures 38-41.

In the case of the conducted analysis concerning the determination of the electrodynamic forces affecting the contacts of the main and arcing contact, the simulation approach presented by the authors may now be one of the simpler and very useful methods for determining the approximate values of the electrodynamic forces. Depending on the accuracy of the 3D model adopted for calculations, the obtained results are much more reliable than simplified analytical methods. In the case of such a complex structure as a high-voltage circuit breaker, and more precisely in the case of the performed analysis of its switching chamber, it is not possible to determine the exact values of the interacting electrodynamic forces in an analytical manner with the use of formulas and simplifications. Even if such computational steps were taken, the obtained results were subject to error and uncertainty.

IX. CONCLUSION

In the performed simulation, authors used an accurate 3D model prepared on the basis of measurements of individual parts of the dismantled pole of the high-voltage circuit breaker. The 3D model obtained in this way allowed for the performance of reliable simulation analyses, which helped to visualize how the contacts of the HV circuit breaker can actually behave in the event of the flow of short-circuit currents and to what electrodynamic exposures those are subjected to.

Interestingly, on the basis of the obtained results, the authors illustrated that the individual contacts of both the main contact and the arcing contact are not evenly electrodynamically loaded. From the generated electrodynamic force waveforms for each contact point, doubts were raised as to the possibility of using simplifications and performing calculations only for 1 contact point, which can be found in the literature. The obtained results show that the values of the electrodynamic forces can differ even from 2 kN, which in turn may initiate the deformation of the contact or even the damage of the whole contact system. Performing this type of numerical analysis on even more accurate 3D models in the form of structural models in R&D departments allows for obtaining precise data on electrodynamic exposures. Each improvement or change in design can be quickly simulated, which in the process of creating a prototype, e.g. of current circuits and contacts of a high-voltage circuit breaker, is extremely important in terms of cost reduction and limiting the number of prototypes for experimental tests in research laboratories.

Authors conducted thorough research of the literature which confirms the lack of information on the study of electrodynamic forces in high voltage contact systems. In the R&D manufacturers departments of contact systems and static breakers, static tests can be found [x]. The works concern only the contact system made of one element, cut in an appropriate manner. Then, outside the circuit breaker chamber, it is possible to conduct tests by pulling out one of the contacts and determining the force statically. It is not a force related to the flow of current. It is a mechanical force obtained through the elasticity of the material, sometimes also by pressure springs.

The authors referred to the global trend in the research of contact systems of high-voltage devices and focused on the correct selection of:

- materials,
- boundary conditions,
- physics issues.

Authors tried to recreate some of the research in laboratory conditions, in a short-circuit laboratory.

REFERENCES

[1] S. Wang, H. Li, and D. Yuan, "Mechanical characteristics analysis of defective transformer windings under short-circuit fault using 3-D FEM," in *Proc. 20th Int. Conf. Electr. Mach. Syst. (ICEMS)*, Sydney, NSW, Australia, Aug. 2017, pp. 1–4.

[2] G. Kadkhodaei, K. Sheshyekani, M. Hamzeh, and S. D. Tavakoli, "Multiphysics analysis of busbars with various arrangements under short-circuit condition," *IET Electr. Syst. Transp.*, vol. 6, no. 4, pp. 237–245, Dec. 2016.

[3] N. Vladimir, I. Ančić, and A. Šestan, "Effect of ship size on EEDI requirements for large container ships," *J. Mar. Sci. Technol.*, vol. 23, no. 1, pp. 42–51, Mar. 2018.

[4] *High-Voltage Switchgear and Controlgear—Part 102: Alternating Current Disconnectors and Earthing Switches*, Standard IEC 62271-102:2012, International Electrotechnical Commission, Geneva, Switzerland, 2018.

[5] *Short-Circuit Currents—Calculation of Effects—Part 1: Definitions and Calculation Methods*, Standard IEC 60865-1:2011, International Electrotechnical Commission, Geneva, Switzerland, 2012.

[6] S. Kulas, Ł. Kolimas, and M. Piskała, "Electromagnetic forces on contacts," in *Proc. 43rd Int. Univ. Power Eng. Conf.*, Padova, Italy, Sep. 2008, pp. 1–4.

[7] Ł. Kolimas, S. Łapczyński, and M. Szulborski, "Tulip contacts: Experimental studies of electrical contacts in dynamic layout with the use of FEM software," *Int. J. Electr. Eng. Educ.*, vol. 1, pp. 1–4, Dec. 2019.

[8] L. Kolimas, S. Łapczyński, M. Szulborski, and M. Świetlik, "Low voltage modular circuit breakers: FEM employment for modelling of arc chambers," *Bull. Polish Acad. Sci. Tech. Sci.*, vol. 68, no. 1, pp. 61–70, Feb. 2020.

[9] Y. Jiaxin, W. Yang, W. Lei, L. Xiaoyu, L. Huimin, and B. Longqing, "Thermal-dynamic stability analysis for the enclosed isolated-phase bus bar based on the subsegment calculation model," *IEEE Trans. Compon., Packag., Manuf. Technol.*, vol. 8, no. 4, pp. 626–634, Apr. 2018.

[10] D. M. Williams, "Human factors affecting bolted busbar reliability," in *Proc. IEEE 62nd Holm Conf. Electr. Contacts (Holm)*, Clearwater Beach, FL, USA, Oct. 2016, pp. 86–93.

[11] J. Yang, Y. Liu, D. Hu, B. Wu, and J. Li, "Transient vibration study of GIS bus based on FEM," in *Proc. IEEE PES Asia–Pacific Power Energy Eng. Conf. (APPEEC)*, Xi'an, China, Oct. 2016, pp. 1092–1095.

[12] D. G. Triantafyllidis, P. S. Dokopoulos, and D. P. Labridis, "Parametric short-circuit force analysis of three-phase busbars—A fully automated finite element approach," *IEEE Trans. Power Del.*, vol. 18, no. 2, pp. 531–537, Apr. 2003.

[13] J. Yang, Y. Liu, D. Hu, B. Wu, B. Che, and J. Li, "Transient electromagnetic force analysis of GIS bus based on FEM," in *Proc. Int. Conf. Condition Monit. Diagnosis (CMD)*, Xi'an, China, Sep. 2016, pp. 554–557.

[14] X. Guan and N. Shu, "Electromagnetic field and force analysis of three-phase enclosure type GIS bus capsule," in *Proc. IEEE PES TD Conf. Expo.*, Chicago, IL, USA, Apr. 2014, pp. 1–4.

[15] I. C. Popa and A.-I. Dolan, "Numerical modeling of three-phase busbar systems: Calculation of the thermal field and electrodynamic forces," in *Proc. Int. Conf. Appl. Theor. Electr. (ICATE)*, Craiova, Romania, Oct. 2016, pp. 1–9.
[16] Y. Jiaxin, W. Ruichao, L. Huimin, B. Longqing, and W. Hongjian, "Research on the calculation methods of enclosed isolated phase bus-bar in short-circuit condition," in *Proc. IEEE 62nd Holm Conf. Electr. Contacts (Holm)*, Clearwater Beach, FL, USA, Oct. 2016, pp. 111–114.
[17] S. W. Park and H. Cho, "A practical study on electrical contact resistance and temperature rise at at the connections of the copper busbars in switchgears," in *Proc. IEEE 60th Holm Conf. Electr. Contacts (Holm)*, New Orleans, LA, USA, Oct. 2014, pp. 1–7.
[18] J. Gatherer and R. L. Jackson, "A multi-variable parametric study on the performance of bolted busbar contacts," in *Proc. IEEE 61st Holm Conf. Electr. Contacts (Holm)*, San Diego, CA, USA, Oct. 2015, pp. 124–131.
[19] F. M. Yusop, M. K. M. Jamil, D. Ishak, and S. Masri, "Study on the electromagnetic force affected by short-circuit current in vertical and horizontal arrangement of busbar system," in *Proc. Int. Conf. Electr., Control Comput. Eng. (InECCE)*, Pahany, Malaysia, Jun. 2011, pp. 1–8.
[20] G. Kadkhodaei, K. Sheshyekani, and M. Hamzeh, "Coupled electric–magnetic–thermal–mechanical modelling of busbars under short-circuit conditions," *IET Gener., Transmiss. Distrib.*, vol. 10, no. 4, pp. 955–963, Mar. 2016.
[21] J. Lei, J.-Y. Zhong, S.-J. Wu, Z. Wang, Y.-J. Guo, and X.-Y. Qin, "A 3-D steady-state analysis of thermal behavior in EHV GIS busbar," *J. Electr. Eng. Technol.*, vol. 11, no. 3, pp. 781–789, May 2016.
[22] M. Krcum, M. Zubčić, and T. Dlabač, "Electromechanical analysis of the medium voltage earthing switch due to short-time and peak withstand current test," *Energies*, vol. 12, no. 16, pp. 1–17, 2019.
[23] *IEC 60609-Short Circuit Current Standard*. Accessed: May 15, 2020. [Online]. Available: https://pdf.wecabrio.com/iec-60609.pdf
[24] R. Bini, B. Galletti, A. Iordanidis, and M. Schwinne, "Arc-induced turbulent mixing in a circuit breaker model," in *Proc. 1st Int. Conf. Electr. Power Equip.-Switching Technol.*, Xi'an, China, Oct. 2011, pp. 375–378.
[25] L. Wang, H. Liu, W. Zheng, C. Ge, R. Guan, L. Chen, and S. Jia, "Numerical simulation of impact effect of internal gas pressure on chamber housing in low-voltage circuit breaker," *IEEE Trans. Compon., Packag., Manuf. Technol.*, vol. 4, no. 4, pp. 632–640, Apr. 2014.
[26] X. Ye, M. T. Dhotre, J. D. Mantilla, and S. Kotilainen, "CFD analysis of the thermal interruption process of gases with low environmental impact in high voltage circuit breakers," in *Proc. IEEE Electr. Insul. Conf. (EIC)*, Seattle, WA, USA, Aug. 2015, pp. 7–10.
[27] M. T. Dhotre, X. Ye, M. Seeger, M. Schwinne, and S. Kotilainen, "CFD simulation and prediction of breakdown voltage in high voltage circuit breakers," in *Proc. IEEE Electr. Insul. Conf. (EIC)*, Baltimore, MD, USA, Jun. 2017, pp. 11–14.
[28] D. Chen, Z. Li, X. Li, L. Ji, and Z. Song, "Simulation of pressure rise in arc chamber of MCCB during its interruption process," in *Proc. 53rd IEEE Holm Conf. Electr. Contacts*, Pittsburgh, PA, USA, Sep. 2007, pp. 43–47.
[29] C. Rumpler, H. Stammberger, and A. Zacharias, "Low-voltage arc simulation with out-gassing polymers," in *Proc. IEEE 57th Holm Conf. Electr. Contacts*, Minneapolis, MN, USA, Sep. 2011, pp. 1–8.
[30] M. Lindmayer, "Complete simulation of moving arc in low-voltage switchgear," in *Proc. 14th Int. Conf. Gas Discharge Appl.*, Liverpool, U.K., Sep. 2002, pp. 318–324.
[31] H. Nordborg and A. A. Iordanidis, "Self-consistent radiation based modelling of electric arcs: I. Efficient radiation approximations," *J. Phys. D, Appl. Phys.*, vol. 41, no. 13, Jul. 2008, Art. no. 135205.
[32] A. Iordanidis and C. M. Franck, "Self-consistent radiation-based simulation of electric arcs: II. Application to gas circuit breakers," *J. Phys. D, Appl. Phys.*, vol. 41, no. 13, 2008, Art. no. 135206.
[33] N. P. T. Basse, R. Bini, and M. Seeger, "Measured turbulent mixing in a small-scale circuit breaker model," *Appl. Opt.*, vol. 48, no. 32, pp. 6381–6391, 2009.
[34] F. P. Incropera, D. P. DeWitt, T. L. Bergman, and A. S. Lavine, *Introduction to Heat Transfer*, 5th ed. Hoboken, NJ, USA: Wiley, 2006.
[35] P. T. Müller, "Macroscopic electro thermal simulation of contact resistances," Bachelor's thesis, Center Comput. Eng. Sci.-Math. Division, RWTH Aachen Univ., Aachen, Germany, 2016.
[36] P. Kumar and A. Kale, "3-dimensional CFD simulation of an internal arc in various compartments of LV/MV Switchgear," in *Proc. ANSYS Converg. Conf.*, Pune, India, Aug. 2016, pp. 236–241.
[37] Y. Wu, M. Li, M. Rong, F. Yang, A. B. Murphy, Y. Wu, and D. Yuan, "Experimental and theoretical study of internal fault arc in a closed container," *J. Phys. D, Appl. Phys.*, vol. 47, no. 50, Dec. 2014, Art. no. 505204.

MICHAŁ SZULBORSKI received the B.S. and M.S. degrees in electrical engineering from the Warsaw University of Technology, Warsaw, Poland, in 2015 and 2018, respectively, and the B.S. degree in power engineering from the University of Warmia and Mazury in Olsztyn, Olsztyn, Poland, in 2016. He is currently pursuing the Ph.D. degree with the Department of Electrical Apparatus, Warsaw University of Technology. He is also an Engineer in the research and development of electrical equipment. In addition, he is an Application Engineer at ANSYS. His current research interest includes the design of electrical apparatus using FEA simulations.

SEBASTIAN ŁAPCZYŃSKI received the Graduate degree from the Warsaw University of Technology, Warsaw, Poland, in 2016, where he is currently pursuing the Ph.D. degree with the Department of Electrical Power Apparatus. He is also an Analyst, an Engineer, and an Editor specializing in the construction of electrical apparatuses, in aspects related to medium and low voltage electrical devices. His research interests include the construction of electrical apparatuses, electromechanical devices, contact systems, the numerical analysis of electrodynamic interactions, and thermal phenomena in current paths by means of finite element method.

ŁUKASZ KOLIMAS received the Graduate and Ph.D. degrees from the Warsaw University of Technology, Warsaw, Poland, in 2005 and 2008, respectively. He has been as the Doctor of Electrical Apparatus with the Warsaw University of Technology, where he is currently a Research Worker with the Division of Electrical Power Apparatus, Protection and Control. He is also a Constructor of low voltage apparatus, an Expert for Polish Centre for Accreditation in terms of short circuit laboratory, and a member of the Polish Agency for Enterprise Development.

MYKHAILO TYRYK received the bachelor's degree in hydropower engineering from the National University of Water and Management Resources Use, Rivne, Ukraine, in 2018, the Graduate degree in electrical engineering from Lviv Polytechnic National University, Lviv, Ukraine, in 2020, and the second Graduate degree in power engineering from the Warsaw University of Technology, Warsaw, Poland, in 2022. He is currently working as a Continuing Airworthiness Engineer with the Warsaw University of Technology.